Chapter 1

PHASE TRANSITIONS AND CRITICAL PHENOMENA

1.1 Thermodynamics and Statistical Mechanics

A system has macroscopic and microscopic properties. Positions, momenta and the quantum number of particles in the system form its microscopic structure. In addition, macroscopic properties of the system such as volume, pressure, temperature, and specific heat can be observed experimentally. Thermodynamics is the study of the macroscopic properties of matter. Statistical mechanics is the study of the behaviour of the system with a large number of degrees of freedom, given the valid laws of its microscopic behaviours [1]. In other words, statistical mechanics studies the relations between microscopic and macroscopic properties according to the investigation of the atomic structure and experimentally observable parameters together. If the thermodynamic characteristics of the system do not change over time, the system is in a thermodynamic equilibrium.

According to the laws of thermodynamics, thermodynamic potentials are defined as the functions of the characteristic natural variables of the system such as temperature T, pressure P, volume V, entropy S, number of particles N, and chemical potential μ [2]. The most important thermodynamic potentials are the total internal energy U(S,V,N), the Gibbs free energy G (T, P, N), the Helmholtz free energy F (T,V,N), and the enthalpy H(S,P,N). All the thermodynamic properties of the system can be found by taking partial derivatives of thermodynamic potentials [3].

$$\partial U = T\partial S - P\partial V + \mu\partial N \tag{1.1}$$

$$\partial H = T\partial S + V\partial P + \mu\partial N \tag{1.2}$$

$$\partial F = -P\partial V - S\partial T + \mu\partial N \tag{1.3}$$

$$\partial G = -V\partial P - S\partial T + \mu\partial N \tag{1.4}$$

1.2 Phase transitions

An analytic region in which the densities of thermodynamic systemss show continuity is called a thermodynamic phase [4]. Phase transition is a change of matter from one phase to another. Some instantaneous changes of macroscopic properties in a system are signs of the phase transition [5]. Phase transitions occur when there is a singularity in the free energy or one of its derivatives [1]. The transitions from liquid to gas, from a normal conductor to a superconductor, or from paramagnet to ferromagnet are common examples.

If there is a finite discontinuity in one or more of the first derivatives of the appropriate thermodynamic potential, the transition is defined as a first-order phase transition [6]. If the first derivatives are continuous but second derivatives are discontinuous or infinite, the transition will be described as higher order, continuous or critical [6].

The critical point T_C is a certain temperature at which the first-order transition ends and the second-order occurs [1]. At that point second derivatives of thermodynamic potentials are discontinuous. The correlation length of the system at the critical temperature becomes infinite. Because of this, one of the elements of the system can be affected from another element which has no closeby interactions or relations with it.

1.3 Classification of phase transitions

1.3.1 Ehrenfest classification

Firstly Ehrenfest suggested classifying the phase transitions according to the degree of the non-analyticity. Consequently the Ehrenfest classification was the first step for grouping the types of the phase transitions. The Ehrenfest classification separates the phase

transitions according to the minimum derivative of the free energy which is discontinuous during the transition. The Ehrenfest classification depends on the discontinuity in the n-th order derivative of the free energy. Therefore in the Ehrenfest classification, in principle, there are higher order transitions (first-order, second-order, third-order, fourth-order…etc).

If the first derivative of the free energy is discontinuous at the transition, due to the Ehrenfest classification it is defined as first-order transition. For instance the solid/ liquid/ gas transitions are first order transitions because of the existence of the discontinuity in density which is the first derivative of the free energy. Second-order phase transitions have a discontinuity in a second derivative of the free energy. For example the ferromagnetic phase transition can be classified as a second-order phase transitions. Because while the magnetization which is the first derivative of the free energy with respect to the applied magnetic field is continuous at the transition, the second derivative of the free energy with respect to the applied magnetic field which is defined as susceptibility shows discontinuity at the transition.

However this classification cannot be adapted to some situations, so Ehrenfest's classification is flawed. Because if a derivative of the free energy diverges in the thermodynamic limit, the Ehrenfest classification is not enough to explain the situation. For example, in the ferromagnetic transition, the heat capacity diverges to infinity.

1.3.2 Modern classification of phase transitions

The phase transitions are separated into two main groups in the modern classification. These two groups are named similarly to the Ehrenfest classes.

The first-order transition which has a discontinuity in the first derivative of the free energy may have a latent heat. The system may absorb or release an amount of energy. Because the transition of the energy cannot suddenly occur, some parts of the system may

have completed the transition and the other parts have not. This situation is defined as mixed-phase regimes. For example during the boiling of water, the total amount of water cannot instantaneously change into the gas phase. Gas phase and liquid phase of the water are observed together at the same time. Many important phase transitions show the mixed-phase regimes such as solid/liquid/gas transitions and Bose-Einstein condensation.

The second class of phase transitions are the continuous phase transitions, also called second-order phase transitions. These have no associated latent heat. Examples of second-order phase transitions are the ferromagnetic transition and the superfluid transition. The phenomena associated with continuous phase transitions are called critical phenomena, due to their association with critical points.

1.4 Order parameter

According to the definition of thermodynamic phase, within each phase the properties of the system are analytic and have their own spatial symmetries [6]. On the other hand, at the phase boundaries between two phases there is a sudden change in the properties of the system and a non-analytic behaviour in the free energy [5]. For instance, in the phase diagram of a ferromagnetic model, there are two phases with different spatial symmetries. In the $T > T_C$ phase region, there is a rotational invariance because of the non-existence of the magnetization. However if the temperature decreases below the critical temperature, at that phase region the magnetization occurs and destroys the rotational invariance. Briefly the rotational symmetry can appear above the critical temperature and disappear below the critical temperature. To investigate the thermodynamics of the system, a new parameter needs to be defined. This new parameter's thermodynamic average becomes zero in one phase called as the "disordered phase" and it is non-zero in the "ordered phase" [5]. This parameter is called the "order parameter", denoted by M. To be a

first-order transition, the order parameter changes discontinuously during the transition at the boundaries [5]. However if the order parameter is a continuous function during the transition, the phase transition is a second-order transition [5]. Some examples of order parameters for some different type of the systems are shown in Table 1.1. Choosing the right order parameter for the system is very important to analyze the characteristics of the system.

Transition	**Order Parameter**
Ferromagnetic	M
Anti-ferromagnetic	Staggered M
Gas-liquid	$V_G - V_L$
Super fluidity	$\int \partial^3 r < \psi >$

Table 1.1: Order Parameters [3]

1.5 Phase Diagrams

At equilibrium, variables of the system are not totally independent from each other. There is a condition equation, f = (P, ρ, T) = 0, between the thermodynamic variables of the system such as pressure P, density ρ, temperature T.

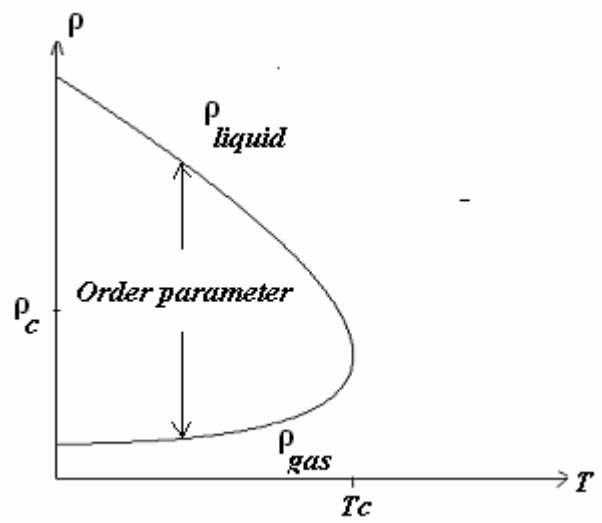

Figure 1.1: Order parameter ($\varphi_{liquid} - \varphi_{gas}$) [1]

The order parameter ($\varphi_{liquid} - \varphi_{gas}$) and the values of the densities along the vapour pressure line are shown in Figure 1.1.

1.6 Examples of phase transitions

The phase diagram of a typical fluid is shown in Figure 1.2. For different temperatures and pressures, water can exist as a solid, a liquid, or a gas. All the phase transitions are first order except at the critical point C [1]. Beyond C it is possible to move continuously from a liquid to a gas.

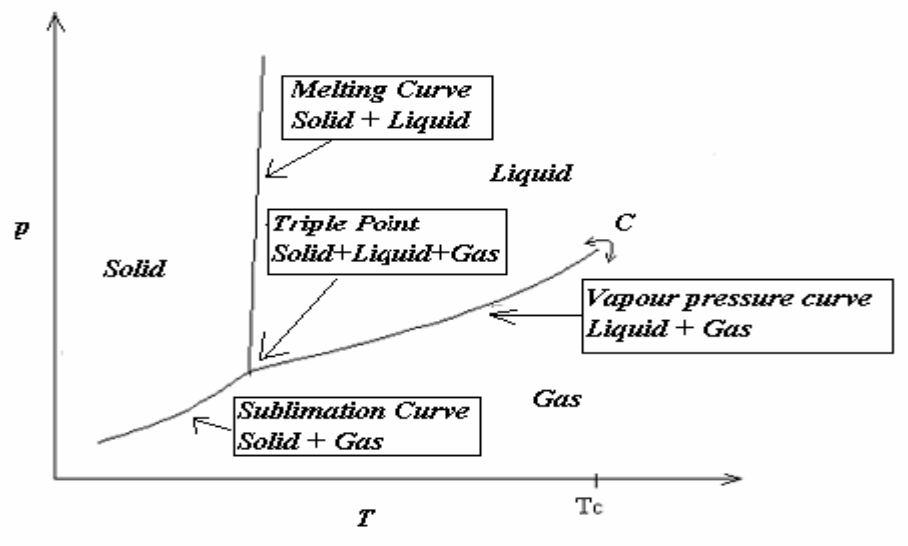

Figure 1.2: Phase diagram of a typical fluid [1]

The phase diagram of a simple ferromagnet is shown in Figure 1.3. There is a first-order transition at zero magnetic field and this transitions come to an end at the critical temperature Tc [1]. After the critical temperature, there is a smooth transition from one phase to another [1].

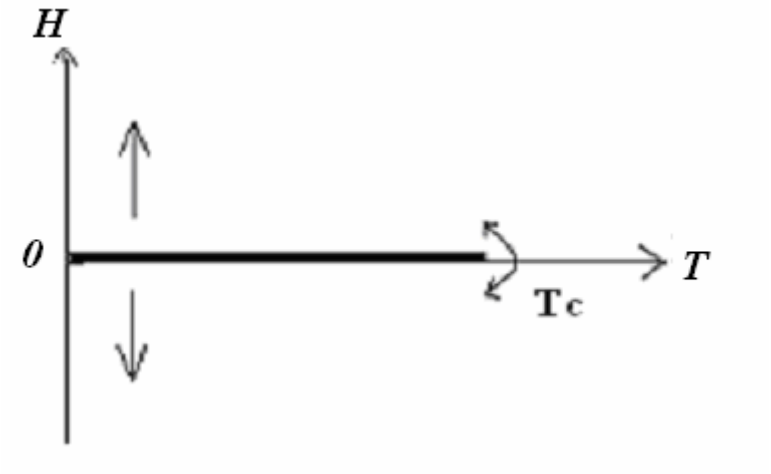

Figure 1.3: Phase diagram of a simple ferromagnet [1]

1.7 Critical-Point Exponents

A phase transition exists at a definite temperature which is called as the critical temperature T_C [2]. To understand the phase transitions, the characteristics of thermodynamic functions of the systems at the critical point have to be investigated. Critical exponents show these characteristics of physical quantities around continuous phase transitions [6]. Critical exponents are independent from some physical properties except the dimension of the system, the range of the interaction, and the spin dimension [5]. The critical exponents can be discovered by using some experimental results. Theoretically, exponents of the higher-dimensional systems (4 or more dimensions) can be calculated by using mean field theory; however for lower-dimensional systems (2 or 3 dimensions) renormalization-group theory gives more successful results.

Specific heat at constant volume V_C : $C_v \sim \lvert t \rvert^{-\alpha}$;
Liquid-gas density difference: $(\rho_l - \rho_g) \sim -t^{\beta}$;
Isothermal compressibility: $\kappa_T \sim \lvert t \rvert^{-\gamma}$;
Correlation length: $\varepsilon \sim \lvert t \rvert^{-\nu}$;
Correlation function at T_C : $G(\vec{r}) \sim 1 / r^{d-2+\eta}$

Table 1.2**:** Critical exponents for a fluid system [1]

Zero-field specific heat:	$C_p \sim \left\|t\right\|^{-\alpha}$;
Zero-field magnetization:	$M \sim (-t)^{\beta}$;
Zero-field isothermal susceptibility:	$\chi \sim \left\|t\right\|^{-\gamma}$;
Correlation length :	$\varepsilon \sim \left\|t\right\|^{-\nu}$;
Correlation function at T_C :	$G(\vec{r}) \sim 1 / r^{d-2+\eta}$

Table 1.3: Critical exponents for a magnetic system [1]

1.8 Equalities of critical exponents

The reduced temperature is defined as $t = \frac{T - T_c}{T_c}$. According to the definition of the reduced temperature at the critical temperature its value becomes zero [2]. The critical exponent is described as $\lambda = \lim_{t \to 0} \frac{\ln\left|F(t)\right|}{\ln\left|t\right|}$ by using the reduced temperature [2]. The equalities between the critical exponents in accordance with their definitions are given below [1].

$$\alpha = 2 - \frac{d}{y_1} \tag{1.5}$$

$$\beta = \frac{d - y_2}{y_1} \tag{1.6}$$

$$\nu = \frac{1}{y_1} = \frac{\ln b}{\ln \lambda} \tag{1.7}$$

$$\gamma = \frac{2y_2 - d}{y_1} \tag{1.8}$$

$$\delta = \frac{y_2}{d - y_2} \tag{1.9}$$

According to these relations;

$$\alpha + 2\beta + \gamma = 2\,, \tag{1.10}$$

and

$$\gamma = \beta(\delta - 1)\,. \tag{1.11}$$

1.9 Symmetry

Generally phase transitions occur between phases with different symmetry. The transition between a fluid and a crystalline solid can be given as an example for the purpose of showing the transition between phases with different symmetry. The arrangements of the atoms in the structure of the fluid are disordered and homogeneous. A continuous translational symmetry is observed in the fluid. In other words, each point inside the fluid has the same properties as any other point. On the other hand, the crystalline solid is composed of atoms arranged in a regular lattice. Each point is not similar to any other points in the lattice.

If there is a phase transition from the more symmetrical phase to the less symmetrical phase, a symmetry breaking is observed. In the transition between the crystalline solid and the fluid, a continuous translation symmetry breaking occurs.

The ferromagnetic transition can be an example of a symmetry-breaking transition. In this type of transition, there is an “up-down symmetry” or “time-reversal symmetry”. There are two reasons for the formation of the symmetry. First of all, for the up-down symmetry, the alignment of the spins in the ferromagnetic phase changes as the direction of the magnetic fields. Secondly, for the time-reversal symmetry, the choice of the time coordinate, which indicates the direction of electric current, is determinative. The symmetry-breaking plays an important role in the characteristics of the phase transitions.

In all the solid-fluid or the ferromagnetic cases, as the temperature is increasing, the system becomes more symmetrical. Whereas the low-energy states are without some of these symmetries, the Hamiltonian of a system usually exhibits all the possible symmetries of the system. This situation is known as spontaneous symmetry breaking. The system is only in the low-energy states at low temperature. However, at higher temperatures, because of the thermal fluctuations, the system can be present at any energy state.

When there is a symmetry-breaking, an extra variable is needed to describe the system. For instance, in the ferromagnetic phase below the Curie temperature, the net magnetization is described by the spin whose direction is chosen spontaneously.

1.10 Universality

The most significant property of critical exponents is being universal. It is possible that systems which are very different from each other can have the same critical exponents [2]. This situation makes them members of the same universality class [2]. This is called universality. In other words, thermodynamic functions of the systems which are in the same universal class show the same behaviours near or at the phase transition [5]. According to the universality property, because of showing the same behaviours, in calculation an easier system can be substituted for a system which is difficult to solve. Investigating the critical

exponents at the critical point is enough to research the behaviours of the systems because the exponents show the characteristics of the derivatives of free energy near the critical point.

1.11 Examples of Universality

Class 1: $YFeO_3$ a ferro magnet, FeF_2 an antiferromagnet, NH_4Cl a molecular crystal, CO_2 and Xe (liquid +gas) fluids, β brass an alloy, 3D Ising model (any lattice) [2].

Class 2: Superfluid helium, planar magnets, and nematic – symmetric liquid crystals

In these classes there are very different substances, however their critical exponents and so their behaviors at T_C are the same [2].

Chapter 2

Scaling Theory of Kadanoff

2.1 Scaling Theory

Kadanoff suggested a new method, which is based on rescaling of the system, for investigating the properties of critical phenomena [7]. The main point of the Kadanoff's scaling is the reduction in the effective number of degrees of freedom [7].

To understand the procedure, the spin-1/2 Ising model can be studied with the Hamiltonian,

$$-\beta H = J\sum_{<ij>} S_i S_j + \mathrm{H}\sum_i S_i \,, \tag{2.1}$$

where <ij> denotes summation over all nearest-neighbor pairs of sites and $S_i = \pm 1$. There is an external magnetic field H on the system. In addition the dimensionality is greater than 1, d > 1. There is an interaction J between the nearest-neighbor spins. For the positive values of J interaction, the alignments of the spins are parallel to each other. The temperature T of the system is proportional to 1/J, so at the low temperatures (means that J is very large) most of the spins become either up ($S_i = +1$) or down ($S_i = -1$). This situation shows the existence of a spontaneous magnetization $\mathrm{M}_0(\mathrm{T})$. Magnetization decreases when T increases. At the critical point where $J = J_C$ and $H = H_C$, the magnetization disappears.

N number of spins constitute the original system with lattice spacing a. According to scaling theory of Kadanoff, spins are grouped into "blocks" as shown in Figure 2.1. The dimensions of blocks are $L \times L \times L \times \cdots \times L$ with L = ba so there are b^d spins in each block. The number of blocks in the system is

$$N' = b^{-d} N \,. \tag{2.2}$$

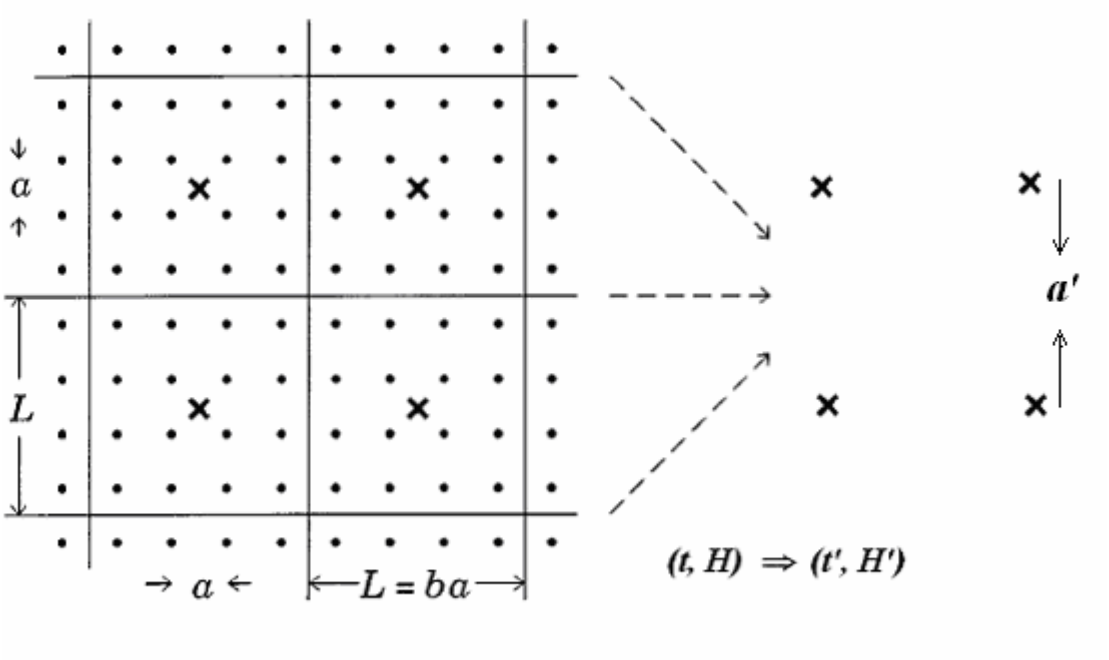

Figure 2.1: Illustration for the scaling theory of Kadanoff

After grouping the spins, the block-spin variable, $S_{i'}^{'}$, which reflects an "important" collective property of the spins inside block, can be described as

$$S_{i'}^{'} = b^{-d} \sum_{i}^{i'} S_i \,. \tag{2.3}$$

The new block-spin variable $S_{i'}^{'} = sign\left(\sum_{i}^{i'} S_i \right) = \pm 1$ at each site i' of the new lattice, so the form of the spins are conserved. The original and the new systems can be made thermodynamically equivalent by the proper choice of (J', H', t'). If these systems are thermodynamically equivalent, the free energies of the systems are equal,

$$-\beta F(t,H) = -\beta F(t',H'), \tag{2.4}$$

and the partition function of each system are equal,

$$\mathrm{Z}(t,H) = Z(t',H'). \tag{2.5}$$

The recursion relations between the original and the new systems are

$$t' = t'(t,H), \tag{2.6.a}$$

and,

$$H' = H'(t,H). \tag{2.6.b}$$

At the critical point, system is scale invariant with the following equations:

$$t' = t'(t = H = 0) = 0 \tag{2.7}$$

$$H' = H'(t = H = 0) = 0 \tag{2.8}$$

and,

$$J' = J'(J = J_C; H = 0) = J_C. \tag{2.9}$$

These recursion relations are analytic. To understand the analyticity, the Taylor expansions of the t' and H' can be written;

$$t' = At + BH \quad \text{and} \quad H' = Ct + DH, \tag{2.10}$$

higher order terms are ignored. There are some conditions because of up-down symmetry;

$$S \to -S \;\Rightarrow\; H \to -H \text{ and } t \to t \;\; (J \to J), \tag{2.11.a}$$

$$S' \to -S' \;\Rightarrow\; H' \to -H' \text{ and } t' \to t' \;\; (J' \to J'), \tag{2.11b}$$

The t' and H' in equation 2.10 can satisfy these conditions only for B=0 and C=0. According to these calculations,

$$t' = b^{y_T} t \,, \tag{2.12}$$

$$H' = b^{y_H} H \,, \tag{2.13}$$

where b is an arbitrary variable. For b=1 (means that there is no rescaling), $t' = t$ and $H' = H$.

2.2 Dimensionless Free Energy per Particle

The free energy per unit particle is a physical quantity that can be calculated either from the original model or the new "rescaled" lattice model. The free energy per particle is

$$f = \frac{1}{N} \ln \mathrm{Z} \tag{2.14}$$

From the conservation of the partition function in equation 2.5, the free energies of the original and rescaled lattice models become equal;

$$Nf(t,H) = N' f(t',H') \quad \Rightarrow \quad Nf(t,H) = Nb^{-d} f(t',H') \,;$$

$$f(t,H) = b^{-d} f(t',H') \,. \tag{2.15}$$

This is the generalized homogeneous function form of the free energy.

2.3 Correlation Length

To investigate the relation between the correlation lengths of the original and rescaled lattice models, the equation of the quantity per unit length can be used;

$$a\zeta(t,H) = ab\zeta(t',H') \quad \Rightarrow \quad \zeta(t,H) = b\zeta(b^{y_T}t, b^{y_H}H). \tag{2.16}$$

2.4 Magnetization

Magnetization, which is the derivative of the free energy with respect to the external magnetic field, is a function of t and H,

$$\mathrm{M}(t,H) = \frac{1}{N}\frac{\partial}{\partial H}\ln \mathrm{Z}(t,H), \tag{2.17}$$

$$\mathrm{M}(t',H') = \frac{1}{N'}\frac{\partial}{\partial H'}\ln \mathrm{Z}(t',H'), \tag{2.18}$$

where $N' = b^{-d}N$ and $H' = b^{y_H}H$. According to the equality of the partition functions of the original and the rescaled lattice models in equation 2.5, the relation between the magnetizations of the models in equations 2.17 and 2.18 can be written

$$\mathrm{M}(t,H) = b^{y_H-d}\mathrm{M}(t',H'). \tag{2.19}$$

The generalized homogeneous function behavior of the magnetization is

$$\mathrm{M}(t,H) = b^{y_H-d}\mathrm{M}'(b^{y_T}t, b^{y_H}H) \tag{2.20}$$

2.5 Internal Energy

The homogeneous function behavior of the energy $U(t,H)$, which is equal to $< S_i S_{i+1} >$, can be found by the equality of the partition function. The derivative of the "lnZ" with respect to coupling constant J gives the energy of the lattice model. The energy of the original system is

$$U =< S_i S_{i+1} >= \frac{1}{N}\frac{\partial}{\partial J}\ln Z(t,H) \tag{2.21}$$

According to the definition of t which equals to $t = \frac{J_C - J}{J_C}$,

$$U = \frac{1}{N}\left(-\frac{1}{J_C}\right)\frac{\partial}{\partial t}\ln Z = \frac{1}{\left(N' b^d\right)}\left(-\frac{1}{J_C}\right)\frac{1}{b^{-y_T}}\frac{\partial}{\partial t'}\ln Z' = b^{y_T - d}\left[\frac{1}{N'}\left(-\frac{1}{J_C}\right)\frac{\partial}{\partial t'}\ln Z'\right] \tag{2.22}$$

$$U(t,H) = b^{y_T - d}U(t',H') \tag{2.23}$$

Generalized homogeneous function behaviors of the energy;

$$U(t,H) = b^{y_T - d}U'(b^{y_T}t, b^{y_H}H) \tag{2.24}$$

2.6 Susceptibility

The magnetic susceptibility is the degree of magnetization of a system in response to an applied magnetic field, represented by χ. In other words, the magnetic susceptibility is the second derivative of the free energy with respect to field.

According to the definition of susceptibility, the relation between the partition function and the susceptibility of the system can be defined by

$$\chi = \frac{\partial}{\partial H}\frac{1}{N}\frac{\partial}{\partial H}\ln \mathrm{Z}. \tag{2.25}$$

The generalized homogeneous function can be found by equations 2.2 and 2.13,

$$\chi = \frac{\partial}{b^{-y_H}\partial H'}\frac{1}{b^{d}N}\frac{\partial}{b^{-y_H}\partial H'}\ln \mathrm{Z}' \tag{2.26}$$

and after rearranging

$$\chi = b^{2y_H - d}\chi'(b^{y_T}t, b^{y_H}H). \tag{2.27}$$

2.7 Specific Heat

Specific heat can be defined by $C_H = \left(\frac{\partial}{\partial t}\langle S_i S_{i+1}\rangle\right)_H$ where $U = < S_i S_{i+1} >$. The generalized homogeneous function form of specific heat can be derived by the equation 2.24,

$$C_H(t,H) = b^{y_T - d}\frac{\partial}{\partial t}U(b^{y_T}t, b^{y_H}H). \tag{2.28}$$

When some arrangements, the function can be written as

$$C_H(t,H) = b^{2y_T-d} C_H(b^{y_T}t, b^{y_H}H). \tag{2.29}$$

2.8 Correlation Function

The correlation function measures how the microscopic variables are correlated with each other. Correlation function can be calculated by

$$\Gamma(r,t,H) = \langle S_0 S_r \rangle - \langle S_0 \rangle \langle S_r \rangle = \frac{\partial}{\partial H_0}\frac{\partial}{\partial H_r}\ln Z, \tag{2.30}$$

$$\Gamma(r,t,H) = \frac{1}{b^{d-y_H}}\frac{\partial}{\partial H_0'}\frac{1}{b^{d-y_H}}\frac{\partial}{\partial H_r'}\ln Z'. \tag{2.31}$$

The generalized homogeneous function form of correlation function is

$$\Gamma(r,t,H) = b^{2y_H-2d}\Gamma(b^{-1}r, b^{y_T}t, b^{y_H}H). \tag{2.32}$$

2.9 The critical exponents

In the generalized homogeneous function forms, b is an arbitrary variable. To calculate the critical exponents, an appropriate b value is chosen in line with the definitions of the critical exponents. The relations between the critical exponents and the thermodynamic properties such as magnetization, susceptibility, specific heat, correlation length are given by

$$M \approx \left|\mathrm{T} - \mathrm{T}_C\right|^{\beta}, \tag{2.33}$$

$$\chi = \frac{\partial M}{\partial H} \approx \left|\mathrm{T} - \mathrm{T}_C\right|^{-\gamma}, \tag{2.34}$$

$$C = \frac{\partial U}{\partial T} \approx \left|\mathrm{T} - \mathrm{T}_C\right|^{-\alpha}, \tag{2.35}$$

$$\zeta \approx \left|\mathrm{T} - \mathrm{T}_C\right|^{-\upsilon}. \tag{2.36}$$

$$M \approx H^{1/\delta} \tag{2.37}$$

$$\Gamma(r) \approx \frac{1}{r^{d-2+\eta}} \tag{2.38}$$

2.9.1 The β exponent

If b is chosen as t^{-1/y_T} in the generalized homogeneous function of magnetization,

$$\mathrm{M}(t,H) = t^{(d-y_H)/y_T}\,\mathrm{M}\left(1, \frac{H}{t^{y_H/y_T}}\right) \tag{2.39}$$

$$\mathrm{M}(t,H) = t^{(d-y_H)/y_T}\, func\left(\frac{H}{t^{y_H/y_T}}\right) \tag{2.40}$$

For the zero external field (H = 0),

$$\mathrm{M}(t,H) = t^{(d-y_H)/y_T}\, func(0). \tag{2.41}$$

When equations (2.33) and (2.41) are compared with each other, then the β exponent can be found

$$\beta = \frac{d - y_H}{y_T}. \tag{2.42}$$

2.9.2 The δ exponent

Similarly if $b = H^{-1/y_H}$, then the scaling form of the magnetization becomes

$$\mathrm{M}(t,H) = H^{(d-y_H)/y_H}\, func\left(\frac{t}{H^{y_T/y_H}}\right) \tag{2.43}$$

From equation (2.37) the δ exponent can be written

$$\delta = \frac{y_H}{d-y_H}. \tag{2.44}$$

2.9.3 The η exponent

To obtain the η exponent, the generalized homogeneous function form of the correlation function is investigated for b = r;

$$\Gamma(r,t,H) = \frac{func(r^{y_T}t, r^{y_H}H)}{r^{2d-2y_H}} \tag{2.45}$$

The η exponent can be found by the comparison of equations (2.45) and (2.38),

$$\eta = d + 2 - 2y_H. \tag{2.46}$$

2.9.4 The ν exponent

At zero-external field, correlation length gives the ν exponent equality. The definition of correlation length exxponent is

$$\zeta = t^{-\nu}\zeta_0 \quad \text{and} \quad \zeta' = (t')^{-\nu}\zeta_0 \tag{2.47}$$

According to the equation 2.12, the equations 2.47 can be rearranged

$$\frac{\zeta}{b} = b^{-1}\zeta_0 t^{-\nu} \quad \text{and} \quad \zeta' = \zeta_0 (t')^{-\nu} = \zeta_0 b^{-y_T \nu} t^{-\nu}. \tag{2.48}$$

The relation between the correlation length of the original and the rescaled system is given in the equation 2.16, $\frac{\xi}{b} = \zeta'$. This equation obtains that $b^{-1} = b^{-y_T \nu_T}$. From this equality

$$\nu_T = 1/y_T. \tag{2.49}$$

Similarly, correlation length for t=0 gives

$$\nu_H = 1/y_H. \tag{2.50}$$

2.9.5 The γ exponent

For $b = t^{-1/y_T}$, γ exponent is obtained with the generalized homogeneous function form of the susceptibility, given by equation 2.27.

$$\chi = t^{(d-2y_H)/y_T}\chi\left(1, \frac{H}{t^{y_H/y_T}}\right) = t^{(d-2y_H)/y_T} func\left(\frac{H}{t^{y_H/y_T}}\right) \tag{2.51}$$

At zero external magnetic field

$$\chi = t^{(d-2y_H)/y_T} func(0). \tag{2.52}$$

According to equation 2.34, the γ exponent can be found as

$$\gamma = \frac{2y_H - d}{y_T}. \tag{2.53}$$

2.9.6 The α exponent

The generalized homogeneous function form of the specific heat with $b = t^{-1/y_T}$ is used to investigate the α exponent;

$$C_H(t,H) = t^{(d-2y_T)/y_T} C_H(1, \frac{H}{t^{y_H/y_T}}) = t^{(d-2y_T)/y_T} func(\frac{H}{t^{y_H/y_T}}) \tag{2.54}$$

$$\alpha = \frac{2y_T - d}{y_T} \tag{2.55}$$

In conclusion, the scaling theory of Kadanoff relates a lattice model with spacing a, and coupling constants J and H, to another lattice model with spacing L=ba, and coupling constants J' and H'. The key assumption of Kadanoff is that both models describe

precisely the same physical system. Therefore, each lattice model has a critical point at the same value, $J = J_C$. However the coupling constants of the lattice models, J and J', are different. One of them is closer to J_C then the other. As a result of this, one lattice model is closer to criticality then the other. The correlation length of the rescaled model is shorter than the original model's, and so rescaled system is further from criticality. However the scaling theory of Kadanoff is very important to study and understand the critical behaviors of the system.

Chapter 3

Renormalization-Group Theory

3.1 The Concepts of the Renormalization-Group Theory

RG theory is based on changing the length scale of a system by removing degrees of freedom [2]. However there are some points at which critical behaviors and properties remain invariant during the rescaling called fixed points [4]. Critical exponents, fixed points, and the other important critical properties can be calculated and explained by using RG theory.

In 1966, Leo P. Kadanoff published a paper which is explained all concepts of rescaling with a real understanding of the physical meaning of the technique [7]. However there were still some points of phase transitions which physicists could not give any explanation. First of all, second-order phase transitions could not be matched through the appropriate universality class according to critical exponents [1]. No calculational method was provided for the recursion relations emerging from rescaling.

After that, with the contributions of Kenneth Wilson in 1971, all the points that could not be explained in the research findings about rescaling theory became clear for physicists [8]. After this revolution, Wilson was awarded the Nobel Prize for this contribution in 1982.

3.2 Definitions of a Renormalization Group Transformation

First of all, the relationship between the Hamiltonian of the original system H and the new Hamiltonian after renormalization H' can be described as

$$\mathrm{H}' = R[\mathrm{H}]. \tag{3.1}$$

Renormalization-group theory changes the number of degrees of freedom from N to N' according to some rules [2]. The principle of renormalization depends on decreasing the number of degrees of freedom and increasing the length scale of the system [1]. At critical points properties of the system do not affect from the rescaling. The scale factor of the transformation, b, is defined by

$$\mathrm{N}' = \frac{\mathrm{N}}{b^{d}}, \tag{3.2}$$

where d is the dimension of the system.

The most important rule for any renormalization-group transformation is to protect the partition function against any change. In other words the partition function must not change under RG transformation [1]. The partitions functions of the original system and the rescaled system are equal to each other.

$$\mathcal{Z}_{N'}(\mathrm{H}') = \mathcal{Z}_{N}(\mathrm{H}). \tag{3.3}$$

Because of rescaling, length, and momentum are changed too. The equation for the length is $\vec{r}' = \frac{\vec{r}}{b}$ and for the momentum $\vec{q}' = b\vec{q}$.

The partition function and the correlation length are determined by the interaction vector K which is a function of temperature. The new interaction vector K' after the transformation can be found by $\mathrm{K}' = R(\mathrm{K})$ which is called the "recursion relation"[2]. In numerical calculations recursion relation is an iteration function. The aim of the RG

transformation is to find the fixed points. To calculate the fixed point, firstly apply the recursion relation for a point many times and after this iteration if the result is the same as the original point, this is a fixed point [1].

$$\mathrm{K}^{*} = R(\mathrm{K}^{*}). \tag{3.4}$$

The new correlation length can be found by

$$\xi(\mathrm{K}') = \frac{\xi(\mathrm{K})}{b}. \tag{3.5}$$

If $\xi(\mathrm{K}^{*})$ does not equal to zero, this means that the correlation length of the original system is infinite [9]. In other words, it is the critical point of the system.

3.3 The Method of Renormalization-Group Theory

To understand the concepts of the renormalization-group theory and to exemplify these concepts, the most common model is the spin 1/2 Ising model in 1 dimension because there is an exact solution for this model with renormalization-group treatment. The Hamiltonian of the model is

$$-\beta H = J\sum_{<ij>} S_i S_j + \mathrm{H}\sum_{i} S_i , \tag{3.6}$$

where <ij> indicates summation over all nearest neighbors in the lattice system.

According to the Figure 3.1, in the renormalization-group transformation while the even numbered spins remain, the odd numbered spins disappear. In the partition function calculations, the even numbered spins are $S_{i'}^{'} = S_i = 2i'$ and the odd numbered spins

are $\sigma_{i'}^{'} = S_i = 2i'-1$. The partition functions of the original and rescaled lattice models, which are shown in Figure 3.1, can be written,

$$Z = \sum_{S_1}\sum_{S_2}\sum_{S_3}\cdots\sum_{S_N} e^{-\beta H\{S\}} = \sum_{\{S'\}}\left(\sum_{\{\sigma'\}} e^{-\beta H\{S',\sigma'\}}\right) = \sum_{\{S'\}} e^{-\beta H'\{S'\}} = Z'. \tag{3.7}$$

To indicate the transformation on one of the group cells, summation over S_3 can be taken as;

$$R(S_2, S_4) \equiv \sum_{S_3} e^{JS_2S_3 + HS_3 + JS_3S_4} = e^{J'S_2S_4 + \tilde{H}(S_2+S_4) + \tilde{G}}, \tag{3.8}$$

where $\tilde{H}$ denotes the external magnetic field contribution to S_2 and S_4 from S_3. Because of being the spin-1/2 Ising model, any spin can be ±1. Therefore after taking the summation over S_3, the equation 3.8 becomes

$$R(S_2, S_4) \equiv e^{J(S_2+S_4)+H} + e^{-J(S_2+S_4)-H} = e^{J'S_2S_4 + \tilde{H}(S_2+S_4) + \tilde{G}} \tag{3.9}$$

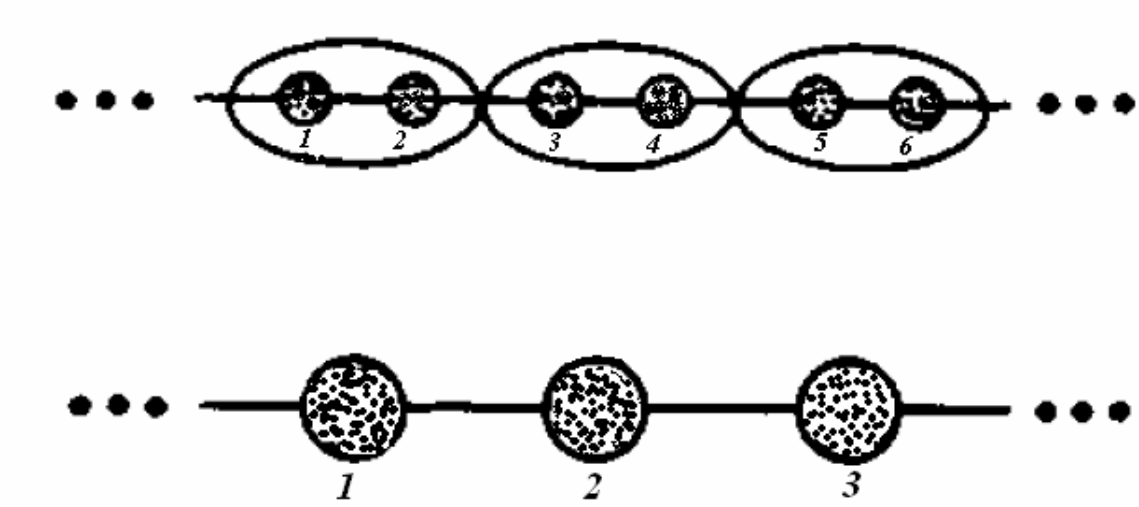

Figure 3.1: Rescaling method of RG theory

For simplicity in the calculations, new definitions can be made as

$$x \equiv e^{J},\ y \equiv e^{H},\ \tilde{g} \equiv e^{\tilde{G}},\ x' \equiv e^{J'},\ \tilde{y} \equiv e^{\tilde{H}}. \tag{3.10}$$

The $R(S_2, S_4)$ function can take different values for different combinations of S_2 and S_4. According to the definition of the $R(S_2, S_4)$ function:

$$R(S_2 = +1, S_4 = +1) = x^2 y + x^{-2} y^{-1} = x' \tilde{y}^2 \tilde{g} \tag{3.11}$$

$$R(S_2 = +1, S_4 = -1) = y + y^{-1} = x'^{-1} \tilde{g} = R(S_2 = -1, S_4 = +1) \tag{3.12}$$

$$R(S_2 = -1, S_4 = -1) = x^{-2} y + x^2 y^{-1} = x' \tilde{y}^{-2} \tilde{g} \tag{3.13}$$

From these equations the $\tilde{g}$, x', $\tilde{y}$ variables, which show the recursion relations, can be calculated,

$$x'^4 = \frac{R(++)R(--)}{R(+-)R(-+)}, \tag{3.14}$$

$$\tilde{y}^4 = \frac{R(++)}{R(--)}, \tag{3.15}$$

$$\tilde{g}^4 = R(++)R(--)R(+-)R(-+). \tag{3.16}$$

There is a H external magnetic field on S_2 and a $\tilde{H}$ contribution from each of the S_1 and S_3 spins. Therefore the external magnetic field after the renormalization becomes

$$H' = H + 2\tilde{H}. \tag{3.17}$$

According to the definition in equation 3.10, $y' = y\tilde{y}^{2}$ and so the renormalized external field can be found by

$$y'^{2} = y^{2}\left((x^{2}y + x^{-2}y^{-1}) \Big/ (x^{-2}y + x^{2}y^{-1}) \right). \tag{3.18}$$

3.3.1 Additive Constant G

An additive constant in the Hamiltonian does not make any physical differences in the properties of the system, but it is useful to the conservation of the partition function. Therefore an additive constant is defined as G.

$$G\sum_{i} 1 = NG. \tag{3.19}$$

The conservation of the partition function with the additive constant can be written as

$$\mathrm{Z} = \sum_{\{S\}} e^{-\beta H + NG} = \sum_{\{S'\}} e^{-\beta' H' + N'G'} = \mathrm{Z}', \tag{3.20}$$

$$f + G = \frac{1}{N}\ln \mathrm{Z} = \frac{1}{b^{d}N}\ln \mathrm{Z}' = b^{-d}(f' + G'). \tag{3.21}$$

If the notation is changed from f to $f^{(0)}$ and from f' to $f^{(1)}$, an iteration equation for free energy can be described as

$$f^{(0)} + G^{(0)} = b^{-dn}(f^{(n)} + G^{(n)}). \tag{3.22}$$

All the singularities are collected into the $G^{(n)}$ term so the free energy becomes soluble. Because of this situation, the additive constant is very important in the renormalization-group theory.

3.3.2 Flow Analysis

The recursion relations can be given by $J' = J'(J,H)$ and $H' = H'(J,H)$. The system is in a closed subspace for H=0 under renormalization-group transformation. Consequently, $H' = H'(J, H = 0) = 0$.

According to the up-down symmetry, $S, S' \to -S, -S'$, $H, H' \to -H, -H'$, and $J, J' \to J, J'$. Fixed points of the systems obtain the following equations;

$$J = J' = J^* \qquad \text{and} \qquad H = H' = H^*. \tag{3.23}$$

There are two fixed points which are shown in Figure 3.2. One of them is a stable fixed point at J = 0 ($T = \infty$), and the other one is an unstable fixed point at $J = \infty$ ($T = 0$). In addition the flows are illustrated in Figure 3.2. For zero external magnetic field, $J' = J'(J, H = 0) = 0$. Thus the recursion relation around the critical point becomes

$$\tanh J' = (\tanh J)^2. \tag{3.24}$$

In Figure 3.2, it is shown that there is a slow flow away from fixed point.

$$e^{-J'} = 2^{1/2} e^{-J} = b^{y_T} e^{-J}, \tag{3.25}$$

where b = 2. This equation gives the critical exponents of the spin-1/2 Ising lattice model. Kadanoff showed that the relation between the reduced temperatures of the original and the rescaled systems as $t' = b^{y_T} t$. According to this equation and the definition of the reduced temperature, the y_T exponent is equal to ½. The ν exponent is given by $1/y_T$, and so ν = 2. In addition, the other recursion relation is $H' = 2H$. According to the scaling theory of Kadanoff, $H' = b^{y_H} H$. Therefore, the y_H exponent is equal to 1. Acoording to the critical exponent equalities,

$$\gamma = {(2y_H - d)}/{y_T} = 2 \qquad \text{and} \qquad \eta = d + 2 - 2y_H = 1 \tag{3.26}$$

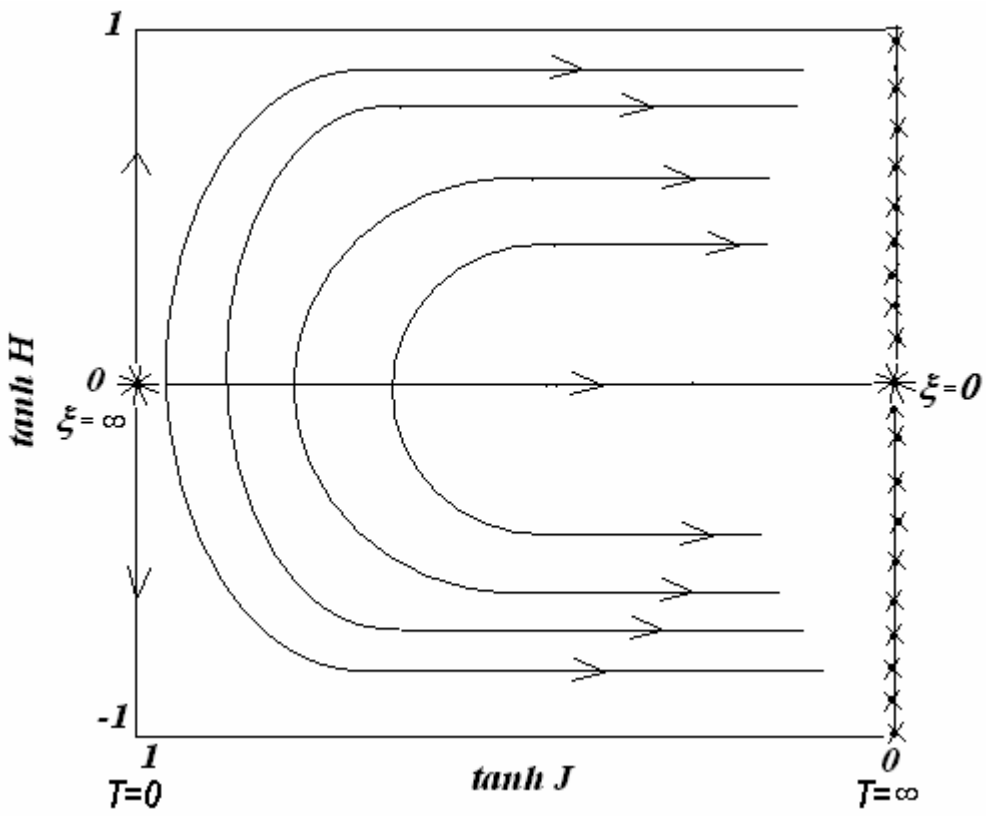

Figure 3.2 The flows of the system.

K. Wilson succeeded in transferring the RG concept from the relativistic quantum field (in particle physics) domain to quite another area of modern theoretical physics. RG theory is applied to study the analysis of phase transition phenomena in spin lattice systems [8], polymer physics [10], noncoherent transfer phenomena [11]. Renormalization-group theory can be used in many physical systems because the solutions are very close to exact experimental results. In addition, according to the universality classes, the critical points and critical exponents of a complex system can be solved with RG transformation by changing the system with a basic one.

Chapter 4

THE BLUME – EMERY – GRIFFITHS MODEL

The Blume-Emery-Griffiths (BEG) model [12, 13] is the most general spin-1 Ising model with the Hamiltonian

$$-\beta \mathrm{H} = J\sum_{<ij>} S_i S_j + K\sum_{<ij>} S_i^2 S_j^2 - \Delta\sum_{<ij>} S_i^2 \,, \tag{4.1}$$

where <ij> indicates summation over nearest-neighbor pairs on the lattice. There are terms of bilinear interaction (J), biquadratic interaction (K), and crystal-field interaction (Δ) in the Hamiltonian of the BEG model. In equation 4.1, the spin $S_i = 0,\pm 1$ is at each site i of a lattice. Each site on the lattice can be either empty $(S_i = 0)$ or occupied by a spin in one of two states $(S_i = \pm 1)$. Generally the BEG model is used for the researches of phase transitions which are constituted by symmetry-breaking fluctuations $(S_i = \pm 1)$ and by density fluctuations $(S_i^2 = 1,0)$. The small magnetic-field effect must also be studied for a complete result of phase transitions of the BEG model,

$$H\sum_i S_i + L\sum \left(S_i S_j^2 + S_i^2 S_j\right). \tag{4.2}$$

4.1 The Construction of The BEG Model

At first the BEG model is introduced for investigating the superfluidity and phase transitions of helium mixtures [12]. Before the presentation of the BEG model, the general

properties of the superfluidity and phase transitions of Helium mixtures are studied by J. Wilks, E. H. Graf, D. M. Lee, and J. D. Reppy [20, 21]. These studies show that in the $He^3 - He^4$ mixtures if the He^3 concentration is less than 67%, the λ transition occurs. However for the higher values of the He^3 concentration, there is a first order transition between the He^3 phase and the He^4 phase. At this phase transition, the He^4 phase is superfluid.

To investigate the superfluidity and phase transitions, M. Blume, V. J. Emery, and R. B. Griffiths presented a model which provides the features of the $He^3 - He^4$ mixtures [12]. The spin-1 Ising model is the simplest microscopic model for superfluidity in $He^3 - He^4$ mixtures, when, at each site i of the lattice, $(S_i = 0)$ represents occupation by a He^3 atom and $(S_i = \pm 1)$ represents occupation by a He^4 atom [12]. In the mixture, there are only two types of Helium atoms. Therefore at each site of the lattice there must be either He^3 or He^4. The expected value for the degree of freedom is 2. However the model shows that the degree of freedom is three because S_i can be equal to 1, 0 or -1. To provide an order parameter for the system, the extra degree of freedom which comes from the sign of S_i is necessary. The superfluid order parameter of the Helium mixture is denoted by the thermal average of the total spin

$$M = N^{-1} \sum_{i}^{N} < S_i > \tag{4.3}$$

where N is the total number of the atoms in the mixture.

The only unphysical property of this model is while the thermal average of the total spin, M, has positive or negative values (means that there is a discontinuity), the phases of the superfluid order parameter of the Helium mixture changes continuously.

In the calculations, the numbers of He^3 and He^4 are computed by

$$N_3 = \sum_i^N (1 - S_i^2), \tag{4.4}$$

$$N_4 = \sum_i^N S_i^2, \tag{4.5}$$

and $N_3 + N_4 = N$.

To indicate the possibility of the phase transition, an extra order parameter is needed. This new extra parameter comes from the concentration of He^3 atoms which is described by

$$\mathrm{X} = \frac{< N_3 >}{N} = 1 - < S_i^2 >. \tag{4.6}$$

The order parameters for the translationally invariant system are $M =< S_i >$ and $\mathrm{X} = 1 - < S_i^2 >$. The superfluid order parameter and the phase transition parameter are indicated with the magnetization ordering, M, and the quadrupolar ordering X.

The Hamiltonian has two terms which occur for the interactions between the components with superfluidity effect and classically, interactions without the superfluidity effect. The first term is

$$\mathrm{H}_S = -J \sum_{<ij>} S_i S_j \tag{4.7}$$

where <ij> denotes summation over all nearest-neighbor pairs of sites. If there is no He^3 atoms, in other words the He^3 concentration is zero, the system becomes the usual

Ising model ($S_i = \pm 1$) and H_S in equation 4.7 becomes the Hamiltonian of the Ising model.

Whereas the first term of the Hamiltonian of the $He^3 - He^4$ mixture shows the superfluidity effect, the second term occurs because of the effect of being a classical liquid mixture. The second term of the Hamiltonian is

$$\mathrm{H}_I = -K_{33}\sum_{<ij>}(1-S_i^2)(1-S_j^2) - K_{44}\sum_{<ij>}S_i^2 S_j^2 - K_{34}\sum_{<ij>}\{S_i^2(1-S_j^2) + S_j^2(1-S_i^2)\} \qquad (4.8)$$

where <ij> indicates summation over all nearest-neighbor pairs of sites and $S_i^2 = 0$ for He^3 and $S_i^2 = 1$ for He^4. In addition $K_{\alpha\beta}$ term denotes the interaction between the He^3 atoms and He^4 atoms. After some arrangements this part of the Hamiltonian becomes

$$\mathrm{H}_I = -(K_{33} + K_{44} - 2K_{34})\sum_{<ij>}S_i^2 S_j^2 - 2q(K_{34} - K_{33})\sum_{i}^{N}S_i^2 - qNK_{33}\,, \qquad (4.9)$$

where q is the number of nearest neighbors on the lattice. The reason of being different $K_{\alpha\beta}$ interactions between He atoms are the differences of mass and statistics. If there are no differences, the $K_{\alpha\beta}$ values are equal and this second term, H_I, of the Hamiltonian is only a constant.

Finally in the Hamiltonian, there are two contributions from the effects of the chemical potentials of the He^3 atoms and He^4 atoms which is described by μ_3 and μ_4. In the end, the Hamiltonian can be written as

$$\mathrm{H} = \mathrm{H}_S + \mathrm{H}_I - \mu_3 N_3 - \mu_4 N_4\,. \qquad (4.10)$$

When the equations 4.4, 4.5, 4.7, 4.8, and 4.9 are placed in the Hamiltonian, it becomes

$$\mathrm{H} = -J\sum_{<ij>} S_i S_j - K\sum_{<ij>} S_i^2 S_j^2 + \Delta\sum_i S_i^2 - N(qK_{33} + \mu_3)\,, \tag{4.11}$$

where $K = K_{33} + K_{44} - 2K_{34}$ and $\Delta = \mu_3 - \mu_4 + 2q(K_{33} - K_{44})$. The last term in the equation 4.11 can be ignored. Therefore the last form of the Hamiltonian can be written as

$$\mathrm{H} = -J\sum_{<ij>} S_i S_j - K\sum_{<ij>} S_i^2 S_j^2 + \Delta\sum_i S_i^2\,. \tag{4.12}$$

The terms on the right-hand side are, respectively, the bilinear exchange, biquadratic exchange, and crystal-field interactions.

4.2 Mean - Field Approximation for The BEG Model

The Gibbs variational principle for the free energy is the best method to study the molecular field approximation. According to the Gibbs variational principle,

$$F = -kT\ln \mathrm{Z} \le Tr\rho\mathrm{H} + kTTr\rho\ln\rho \equiv \psi(\rho) \tag{4.13}$$

where F is the exact free energy and ρ is any density matrix. This density matrix has three important features. Firstly, it is a hermitian matrix (means that it is equal to its own conjugate transpose). Then it is a non-negative matrix (means that all the eigenvalues of the matrix are non-negative). Finally, the summation of the eigenvalues of the density matrix is equal to 1,

$$Tr\rho = 1\,. \tag{4.14}$$

The equality in the Gibbs variational principle holds when

$$\rho = \frac{e^{-\beta \mathrm{H}}}{Tre^{-\beta \mathrm{H}}} = \rho_{canonical} \ . \tag{4.15}$$

At the lattice, there are N spins and all spins are located at each i site of the lattice. In the mean-field approximation each spin has its own density matrix, which is called single-spin density matrix, denoted by ρ_i. The relationship between the general density matrix of the system and single-spin density matrix is

$$\rho = \prod_{i}^{N} \rho_i \ . \tag{4.16}$$

When the equations 4.12, 4.16 are put into the equation 4.13,

$$\psi = Tr \prod_{i'} \rho_{i'} \left\{ -J \sum_{<ij>} S_i S_j - K \sum_{<ij>} S_i^2 S_j^2 + \Delta \sum_i S_i^2 \right\} + \frac{1}{\beta} Tr \prod_{i'} \rho_{i'} \left(\ln \prod_i \rho_i \right) \tag{4.17}$$

$$\psi = -J \sum_{<ij>} \left(tr \rho_i S_i \right) \left(tr \rho_j S_j \right) - K \sum_{<ij>} \left(tr \rho_i S_i^2 \right) \left(tr \rho_j S_j^2 \right) + \Delta \sum_i \left(tr \rho_i S_i^2 \right) + \frac{1}{\beta} Tr \prod_{i'} \rho_{i'} \left(\sum_i \ln \rho_i \right) \tag{4.18}$$

To provide a translationally invariant system, density matrices (ρ_i and ρ_j) must be independent from the locations of sites, so in the calculation they become as ρ_1. In addition, instead of the summations which are over all the nearest neighbors in the calculations, the $\frac{1}{2} qN$ factor comes because of the nonexistence of the i-site dependence. Therefore the following step is,

$$\psi = -\left(\frac{1}{2}qN\right)J\left(Tr\rho_1 S_1^2\right) - \left(\frac{1}{2}qN\right)K\left(Tr\rho_1 S_1^2\right)^2 + \Delta N\left(Tr\rho_1 S_1^2\right) + N\frac{1}{\beta}Tr\rho_1 \ln \rho_1 . \quad (4.19)$$

When the left-hand side and the right-hand side of the equation 4.19 are divided by N,

$$\frac{\psi}{N} = -\frac{1}{2}\hat{J}\left(Tr\rho_1 S_1^2\right) - \frac{1}{2}\hat{K}\left(Tr\rho_1 S_1^2\right)^2 + \Delta\left(Tr\rho_1 S_1^2\right) + \frac{1}{\beta}Tr\rho_1 \ln \rho_1 , \quad (4.20)$$

where $\hat{J} = qJ$ and $\hat{K} = qK$.

The best and the most appropriate form of the single-site density matrix, ρ_1 is the one which minimizes the $\frac{\psi}{N}$ value. After differentiating $\frac{\psi}{N}$ in equation 4.20 with respect to ρ_1, the single-site density matrix can be found as

$$\rho_1 = \frac{e^{-\beta\overline{H}}}{Tre^{-\beta\overline{H}}} \quad (4.21)$$

where $H_1 = -\hat{J}(Tr\rho_1 S_1)S_1 - \hat{K}(Tr\rho_1 S_1^2)S_1^2 + \Delta S_1^2$. According to the definitions of the two order parameters $M = < S_i >$ and $\mathrm{X} = 1 - < S_i^2 >$, the equation 4.21 can be written as

$$H_1 = -\hat{J}\mathrm{M}S_1 - \left[\Delta - \hat{K}(1-\mathrm{X})\right]\Delta S_1^2 \quad (4.22)$$

where

$$\mathrm{M} = \frac{2\sinh \beta\hat{J}\mathrm{M}}{\exp(\beta\{\Delta - \hat{K}(1-\mathrm{X})\}) + 2\cosh \beta\hat{J}\mathrm{M}} \quad (4.23)$$

and $$1-\mathrm{X}=\frac{2\cosh\beta\hat{J}\mathrm{M}}{\exp(\beta\{\Delta-\hat{K}(1-\mathrm{X})\})+2\cosh\beta\hat{J}\mathrm{M}}\ . \qquad (4.24)$$

Generally X has an exact value in a mixture so the Δ and M can be calculated from the equations 4.23 and 4.24. According to these assumptions, the X and M can be calculated from the equations 4.23 and 4.24. There are two types of solutions. The first solution for the X and M values is

$$1-\mathrm{X}=\frac{2}{\exp(\beta\{\Delta-\hat{\mathrm{K}}(1-\mathrm{X})\})+2}\quad\text{and}\quad \mathrm{M}=0, \qquad (4.25)$$

and the other solution is

$$1-\mathrm{X}=\mathrm{M}\coth\beta\hat{J}\mathrm{M}\qquad\text{and}\quad \mathrm{M}\neq 0\,. \qquad (4.26)$$

In the study of M. Blume, V. J. Emery, and R. B. Griffiths, the phase diagrams of the BEG model are examined for two different cases, in the first case $\hat{K}=0$ and in the other case $\hat{K}\neq 0$. In the calculations, the general regions of phases in which magnetization is either zero or nonzero, can be found by the equations 4.25 and 4.26. However the phase transition lines between the phases must be calculated analytically. The characteristics of the phase transition line are very different for $\hat{K}=0$ and $\hat{K}\neq 0$ cases.

4.2.1 Case 1: $\hat{K} = 0$:

In this case first of all, to obtain a nonzero magnetization, it is assumed that the system is in a small magnetic field. Because of this magnetic field, hence there must be ($\hat{J}\mathrm{M} - H$) term in every equation which includes the $\hat{J}\mathrm{M}$.

The thermodynamic potential G(M) is given by

$$G(\mathrm{M}) = \psi - \mathrm{MH} \quad \text{and} \quad \mathrm{H} = -\frac{\partial G}{\partial \mathrm{M}}. \tag{4.27}$$

If the magnetic field, H=0 the thermodynamic potential, G(M) has its minimum value with respect to M. The thermodynamic potential G can be expanded in powers of M

$$G = G_0 + AM^2 + BM^4 + CM^6 + ..., \tag{4.28}$$

which has the form the Landau's theory of phase transitions. In this case $\hat{K} = 0$ and the magnetization $M \neq 0$ because of $\mathrm{H} \neq 0$. Therefore the equation 4.23 becomes

$$\mathrm{M} = \frac{2\sinh\beta(\hat{J}\mathrm{M} - \mathrm{H})}{e^{\beta\Delta} + 2\cosh\beta(\hat{J}\mathrm{M} - \mathrm{H})} \quad . \tag{4.29}$$

According to equation 4.27 the external magnetic field can be written as

$$\mathrm{H} = -2A\mathrm{M} - 4B\mathrm{M}^3 - 6C\mathrm{M}^5 - ..... \tag{4.30}$$

When the equation 4.29 is expanded, H can be found as a series in powers of M and if it is compared with the equation 4.30, the A, B, C constants can be written,

$$A = \frac{\delta}{2\beta} - \frac{1}{2}\hat{J} \quad , B = \frac{1}{8\beta}\left(\delta^2 - \frac{1}{3}\delta^3\right), \text{ and } \quad C = \frac{1}{6\beta}\left(\frac{1}{2}\delta^3 - \frac{3}{8}\delta^4 + \frac{3}{40}\delta^5\right), \qquad (4.31)$$

where $\delta = 1 + \frac{1}{2}e^{\beta\Delta}$.

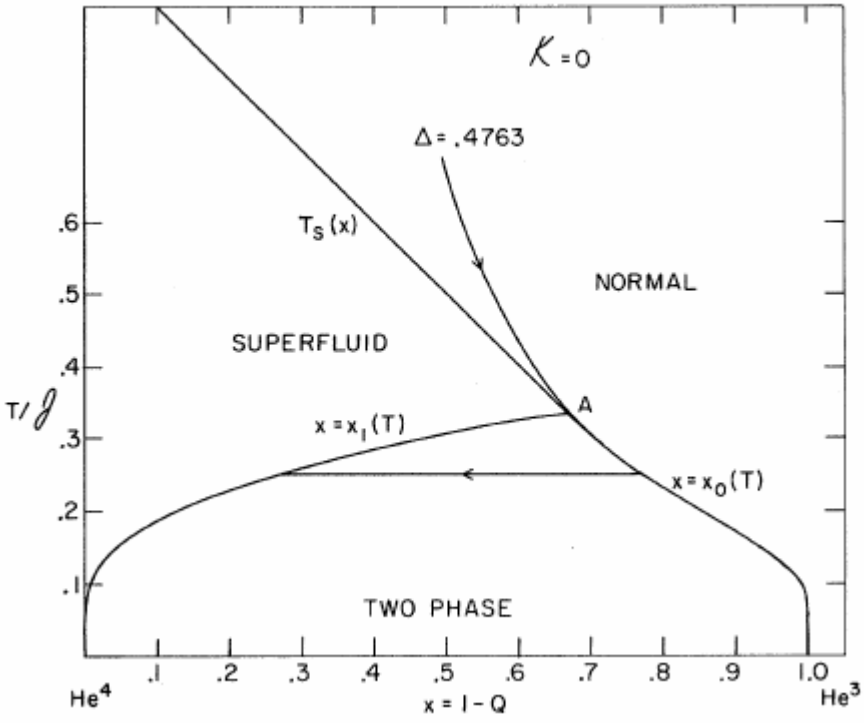

Figure 4.1: BEG phase diagram for Helium mixtures obtained with the mean-field approximation for $\hat{K} = 0$ [12].

According to equation 4.27, for H=0, G is a minimum with respect to M. For A>0 and B>0, at M=0, the minimum is observed. However for the negative values of A, the maximum occurs at M=0. Eventually when A=0 there is a superfluid ordering temperature which is shown as $T_S(X)$. From the definition of the constant A at equation 4.31, it is found that $A = \frac{\delta}{2\beta_s} - \frac{1}{2}\hat{J} = 0 \Rightarrow \frac{1}{\delta} = \frac{1}{\beta_s \hat{J}} = \frac{1}{\left(1/T_S\right)\hat{J}} = \frac{T_S}{\hat{J}}$ and from the first solution set in the equation 4.25, it is found that $1 - X = \frac{2}{\exp(\beta\Delta) + 2} \Rightarrow \frac{1}{1-X} = \frac{1}{2}e^{\beta\Delta} + 1 = \delta$. From these calculation the superfluid ordering temperature can be written as

$$\frac{T_S(X)}{\hat{J}} = 1 - X . \tag{4.32}$$

Specially, according to the equation (4.32) for X=0 (means that there is only He^4 in the system), the superfluid ordering temperature is equal to $\hat{J}$; $T_S(X=0) = \hat{J}$. As the value of X which shows the concentration of He^3 in the system, is increased, the superfluid ordering temperature decreases linearly from the $T_S(X=0) = \hat{J}$ value. The $T_S(X)$ temperature line is shown in the Figure 4.1. While the constant A is zero, at the critical values of the X and T, the other constant B becomes zero. From that point, the phase transition becomes first-order. According to the definition of B in equation 4.31 and the definition of the $T_S(X)$ temperature in equation 4.32, the critical temperature can be calculated as

$$\frac{T_C}{T_S(0)} = 1 - X_C = \frac{1}{3} \tag{4.33}$$

Before A becomes to equal zero, the thermodynamic potential G(M) has two minimum points, at M=0 and M_0 with the same free energy, as T decreased, for $\Delta > \Delta_C$. The zero magnetization is related with the He^3 phase.

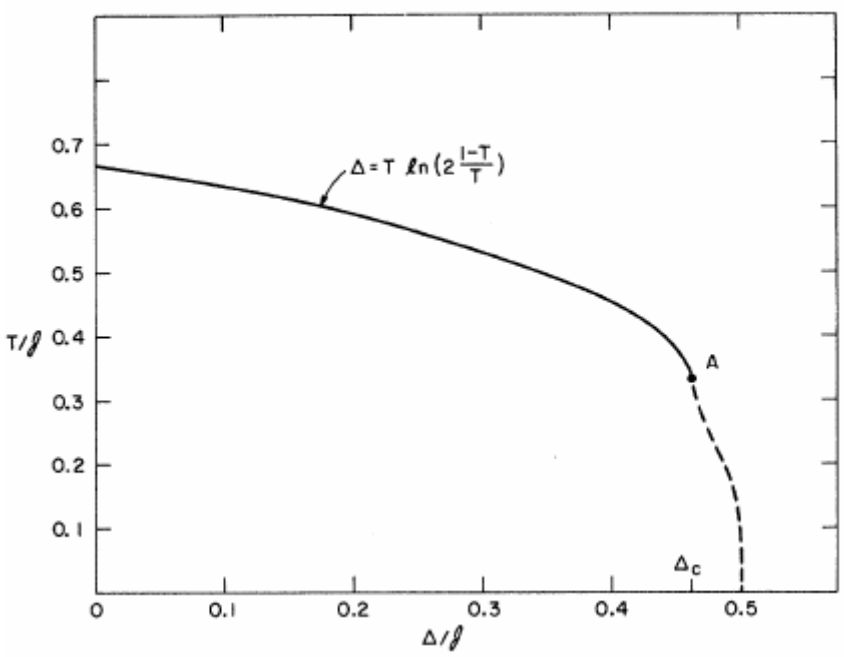

Figure 4.2: Phase diagram for $\hat{K} = 0$ in the T-Δ plane, obtained by mean-field approximation. Dashed and solid lines, respectively, indicate the first-order transition and the second-order transition. The tricritical point is shown by A. [12].

Phase diagram in the T- Δ plane with $\hat{K} = 0$ is shown in Figure 4.2. The He^4 concentration shows the superfluity and for pure He^4, the superfluid ordering temperature $T_S(X = 0) = \hat{J}$ and $\Delta = -\infty$. Therefore the second-order transition, in other words

superfluid ordering, occurs at $T = \hat{J}$ and $\Delta = -\infty$ values. The tricritical point shows the end of the second order transition and the starting point of the first-order transition, denoted by A in the Figure 4.2. At the tricritical point, $\Delta_C = \left(\frac{2}{3}\ln 2\right)\hat{J} = 0.4621\hat{J}$ and $T_C = \frac{1}{3}\hat{J}$.

4.2.2 Case 2: $\hat{K} \neq 0$:

In this case, phase diagrams are investigated for some different values of the $\hat{K}$ interaction. Griffiths showed that the system gives the same features of the spin-1/2 Ising model for $\hat{J} = 0, \hat{K} > 0$ [22]. The phase diagram of this situation is shown in Figure 4.3(a). Because of being more attractive than $He^3 - He^4$ interaction, the $He^3 - He^3$ and $He^4 - He^4$ interactions are the reasons of the phase separation.

There are three situations according to the $\hat{K}/\hat{J}$ value. Firstly, for small values of $\hat{K}/\hat{J}$, the superfluid phase transition occurs from second order to first order, described by case 1. For large values of $\hat{K}/\hat{J}$, the reason of the superfluid transition is the interactions, exemplified by Figure 4.3(c) and 4.3(d). For intermediate values of $\hat{K}/\hat{J}$, the direction of the line of constant Δ guides to the transition. In Figure 4.1 the line of constant Δ comes from right to left. However, in Figure 4.3(a), the direction is from left to right.

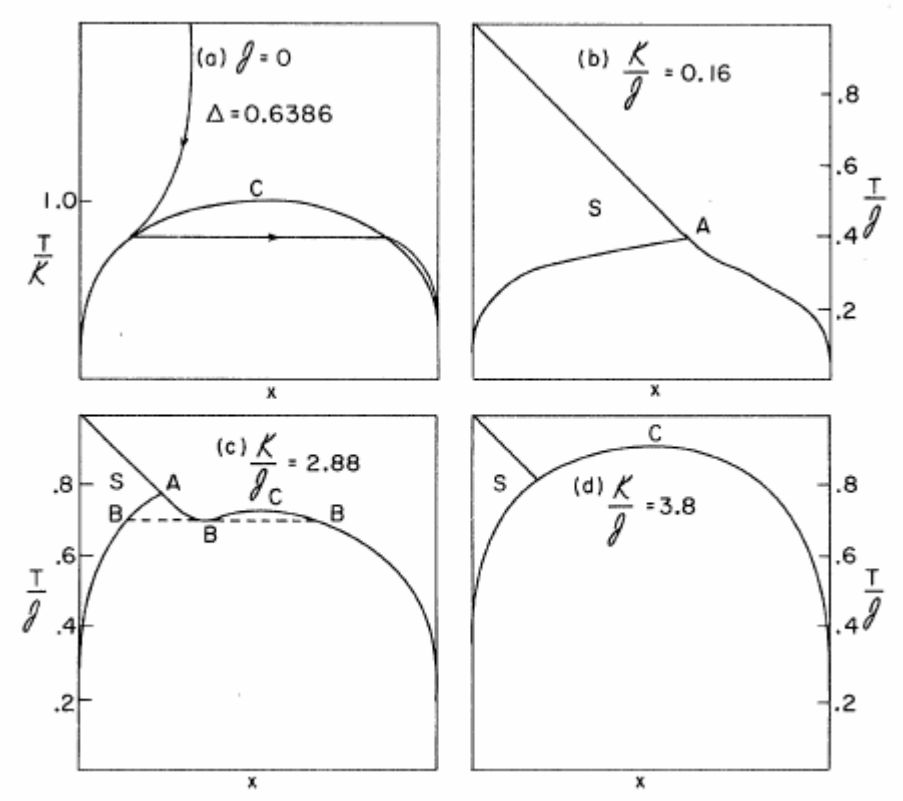

Figure 4.3: Phase diagrams for $He^3 - He^4$ mixtures as predicted by the mean-field approximation with some different $\hat{K}$ values. Superfluid phases are indicated by S [12].

The crossing point between the λ-line and the phase transition curve is given by

$$\frac{\mathrm{T}_C}{\mathrm{T}_S(0)} = 1 - \mathrm{X}_C = \frac{2\hat{K}+1}{2\hat{K}+3}. \tag{4.37}$$

In Figure 4.3, it is shown that as $\hat{K}/\hat{J}$ is increased, the tricritical point starts to slide to the left. The characteristics of the large $\hat{K}/\hat{J}$ can be seen obviously in the phase diagram when $\hat{K}/\hat{J}$ is increased enough. In Figure 4.3(a), there is no λ transition and the reason of the phase transition is the interactions between particles. A small change in the value of $\hat{K}/\hat{J}$ makes the phase diagram, in Figure 4.3(b), similar to the one which is shown in Figure 4.1. As $\hat{K}/\hat{J}$ value is increased further, a critical point and a tricritical point occur in the phase diagram. In addition to this, a triple point occurs. This is interesting because these points are observed at three different concentrations while the temperature is constant. If the $\hat{K}/\hat{J}$ value is increased still further, the tricritical point disappears and the λ-line meets the phase transition curve below the critical point C which is the maximum of the phase transition curve.

The continuity in the slope of the λ line $\mathrm{T}_S(\mathrm{X})$ still occurs even if the existence of a nonzero $\hat{K}/\hat{J}$ value. As in case 1, this is a result of molecular field approximation. The phase diagrams in the T-Δ plane are shown in Figure 4.4. As $\hat{K}/\hat{J}$ is increased, for a small change, the critical point C in Figure 4.4(a) disappears and a tricritical point A occurs which is exemplified by Figure 4.4(b). As $\hat{K}/\hat{J}$ is increased further, a tricritical point, a critical point and a triple point occurs, shown in Figure 4.4(c). If $\hat{K}/\hat{J}$ is increased still further, the tricritical point disappears. In addition between the superfluid phase and the normal phase there is only a second-order transition in this situation.

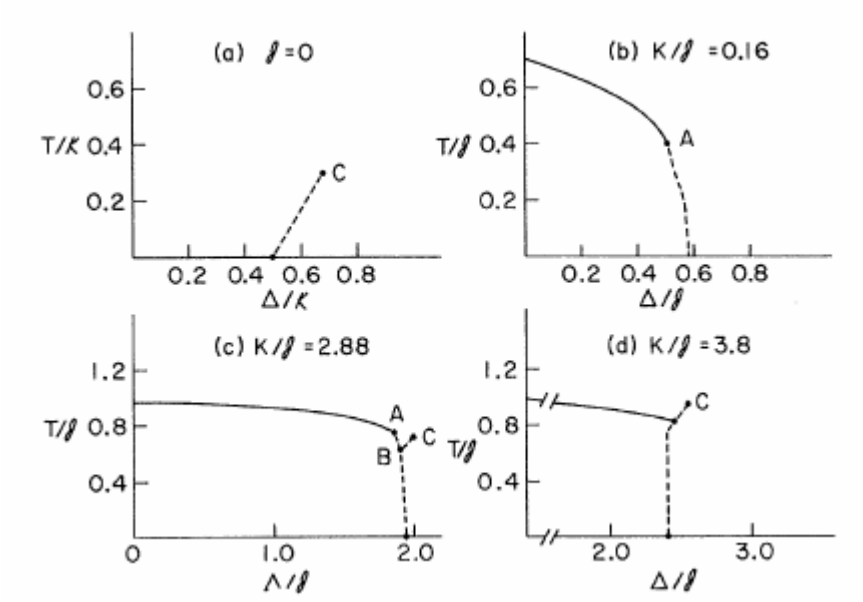

Figure. 4.4: Phase diagrams for $\hat{K} \neq 0$ in T-Δ plane. Solid lines Represents the second-order transitions, dashed lines show first-order transitions. The critical point, the tricritical point and the triple point are, respectively, denoted by C, A, B. [12]

In this study M. Blume, V. J. Emery, and R. B. Griffiths present a simple spin-1 Ising model which explains the characteristics of some important thermodynamic properties. The BEG model is used to investigate the superfluid-normal transitions in helium mixtures. Global phase diagrams and critical points of the BEG model for positive values of J and K interactions are studied by mean-field theory [12]. The results of this simple model are well-matched with the experimental results.

4.3 Phase Diagrams of The BEG Model: Renormalization-Group Theory

4.3.1 Case 1: Phase diagrams for the positive values of J and K interactions

In spite of the Hamiltonian's simple form, the global phase diagrams are quite complex because of providing a rich variety of phase transition phenomena, with first- and second-order phases transitions, bicritical, tricritical and other multicritical transitions. After the study of M. Blume, V. J. Emery, and R. B. Griffiths, the BEG model for positive values of J and K interactions are studied by renormalization-group transitions [13].

A. N. Berker and M. Wortis are studied the BEG model in two dimensions with a position-space renormalization-group transformation. The magnetic-field effects must be considered for an exact result of phase transitions of the BEG model,

$$H\sum_i S_i + L\sum\left(S_i S_j^2 + S_i^2 S_j\right). \tag{4.38}$$

First of all, the exact information on the phase diagram of the BEG model is necessary to interpret and analyze the results of the study which is found by the position-space renormalization-group (PSRG) method. The two order parameters of the BEG model are the magnetization and the quadrupole order parameter as described in the study of M.

Blume, V. J. Emery, and R. B. Griffiths [12]. In J, K, and Δ space, the order parameters can be written,

$$\mathrm{M}(J,K,\Delta) \equiv < S_i > = \mathrm{Z}^{-1} \sum_{\{S\}} S_i e^H \ , \tag{4.39}$$

$$Q(J,K,\Delta) \equiv < S_i^2 > = \mathrm{Z}^{-1} \sum_{\{S\}} S_i^2 e^H \ , \tag{4.40}$$

where {s} indicates summation over all spin configurations and the usual –β term is taken into the Hamiltonian, denoted by H. For a translationally invariant system, S_i must be independent of i. Therefore the partition function of the system can be formulized as

$$\mathrm{Z}(J,K,\Delta) = \sum_{\{S\}} e^H \ . \tag{4.41}$$

Exact Information 1

The exact result for the two dimensional spin-1/2 Ising model is given by Onsager. If the two dimensional spin-1/2 Ising model is compared with the BEG model, some important points can be clearly understood. In the BEG model, all spin configurations are nonzero, $\{S_i = \pm 1\}$ at Δ<<-1. These spin configurations govern the order parameters in equations 4.39 and 4.40. For $\{S_i = \pm 1\}$, the Hamiltonian of the system can be calculated as

$$\mathrm{H}(J;\{S\}) = J \sum_{<ij>} S_i S_j + K - \Delta \, . \tag{4.42}$$

The second term and the third term can be ignored because they are only some constants in the Hamiltonian. Therefore the Hamiltonian becomes

$$\mathrm{H}(J;\{S\}) = J\sum_{<ij>} S_i S_j \ . \tag{4.43}$$

That is the same Hamiltonian of the two dimensional spin-1/2 Ising model. The Onsager exact result shows that there is a second-order phase transition at $J = J_{1/2}$. Because of this result, a second-order phase transition is expected at $J = J_{1/2}$ in the phase diagram of the BEG model. Consequently, at $J = J_{1/2}$ there must be a segment of critical surface for the $\Delta<<-1$ and K>0 region which is parallel to J=0 plane. This planar segment of critical transition surface is shown in Figure 4.5, indicated by C. There are two low temperature ferromagnetic phases which are observed with either $\mathrm{M} < 0$ and Q=1 or $\mathrm{M} > 0$ and Q=1 above the critical planar segment, shown in Figure 4.5. Additionally, in Figure 4.5, under the critical surface there is a paramagnetic phase with M=0 and Q=1.

At $\Delta>>1$ for the finite values of J and K interactions, the $\{S_i = 0\}$ configuration dominates the magnetization and the quadrupole order parameter. Eventually the M and Q values become zero.

Exact Information 2

In the $2(J + K) \sim \Delta >>1$ region, there are two possibilities of the spin configurations which dominates the ensemble averages in equations 4.39 and 4.40. First one is the configuration in which all spins are zero, $\{S_i = 0\}$, and the other one is the configuration in which all spins are nonzero, $\{S_i = \pm 1\}$. The respective Hamiltonians for the configurations are

$$H(\{S_i = 0\}) = 0 \ , \tag{4.44a}$$

$$H(\{S_i = S_j = ... = \pm 1\}) = N[2(J+K) - \Delta], \quad N \to \infty , \tag{4.44b}$$

where N is the number of sites on the lattice and it goes to infinity in the thermodynamic limit. Because of this situation, at $2(J+K) = \Delta >> 1$ region, the alignment of the spins changes from the zero configuration to the aligned configuration. This dominant configuration changing causes to a first-order transition between a paramagnetic phase (M=Q=0) at $2(J+K) < \Delta$ and two coexisting ferromagnetic phases (M= ±1, Q= 1) at $2(J+K) > \Delta$. In the $2(J+K) = \Delta$ region, there is a three-phase coexistence which is shown in Figure 4.5 by the plane F_3.

Exact Information 3

Griffiths showed that the energy of a configuration remains same when the S_i term is converted to $-S_i$ in the Hamiltonian at J=0 plane. To understand this feature, a new variable σ_i at each site i is described by

$$\sigma_i = 2S_i - 1 = \pm 1 . \tag{4.45}$$

According to these definition, $S_i = \frac{\sigma_i + 1}{2}$ and after substitute this equation into the Hamiltonian of the BEG model at J=0, the Hamiltonian can be written

$$\mathrm{H}_t(J_t, H_t; \{\sigma_i\}) = J_t \sum_{<ij>} \sigma_i \sigma_j + H_t \sum_i \sigma_i , \qquad \sigma_i = \pm 1 \tag{4.46}$$

where $J_t = \frac{1}{4}K$ and $H_t = K + \frac{1}{2}(\ln 2 - \Delta)$. This simple form shows that the model again reduces to the spin-1/2 Ising model at J=0. However this time, there is an external magnetic

field H_t. It is known that the phase transitions of the spin-1/2 Ising model occur at zero magnetic field (H_t=0). Therefore at J=0 plane, the phase transitions occur along the line $\Delta = 2K + \ln 2$, indicated SF_2 in Figure 4.5. From all of this information, the conditions of the Onsager critical transition are

$$J_G = 0, \quad K_G = 4J_{1/2} \quad \text{and} \quad \Delta_G = 8J_{1/2} + \ln 2. \tag{4.47}$$

The Griffiths-Onsager critical point provides these conditions, indicated by G in Figure 4.5. For $K > K_G$ region, a first order transition between two paramagnetic phases is observed along the line G F_2 in Figure 4.5.

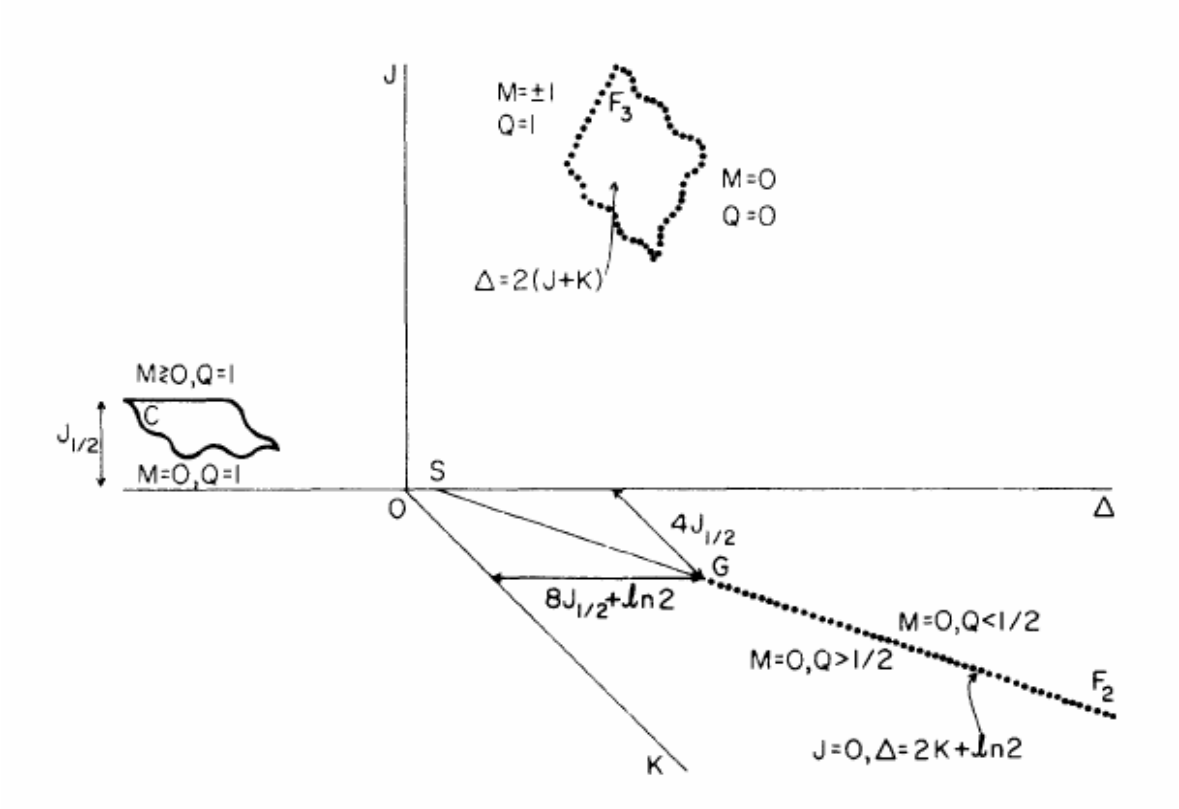

Figure 4.5: Some exact information on the BEG phase diagram [13]. The planar segments of the second-order and the first order transitions are, respectively, indicated by C and F_3. Along the GF_2 line there is a first-order transition and G is the Griffiths-Onsager critical point.

Mean-Field Theory

Mean-field theory suggests that each spin sees the average value of its own neighbors. Furthermore all correlated fluctuations are ignored. The exact information about the phase diagrams of the BEG model can be collected by mean field approximation. The phase diagram with all exact information is obtained with mean-field approximation in Figure 4.6.

In the Figure 4.6, critical and first-order transitions are respectively shown by full lines and dotted lines. Wavy lines represent surface continuity. The critical surface CT_0E_3L and the first order surfaces ($F_3T_0E_3L$ and F_2GE_2L) separate the two coexisting ferromagnetic phases (M > 0 and M < 0) and each of the two paramagnetic phases ((M= 0, Q<1/2) and (M= 0, Q>1/2)). There is three-phase coexistence in the $F_3T_0E_3L$ surface and two-phase coexistence in the F_2GE_2L surface. The intersection lines between these surfaces are the ordinary tricritical line (T_0E_3), the isolated critical line (GE_2) and the critical end line (E_3L) in the phase diagram. E_2 and E_3 are, respectively, critical and tricritical end points. Along the line E_2E_3, there is a four-phase coexistence.

Figures 4.6 and 4.7 include all the conditions of the exact information and the properties of Figure 4.5. This phase diagram can be compared with the diagram which is obtained by renormalization-group theory.

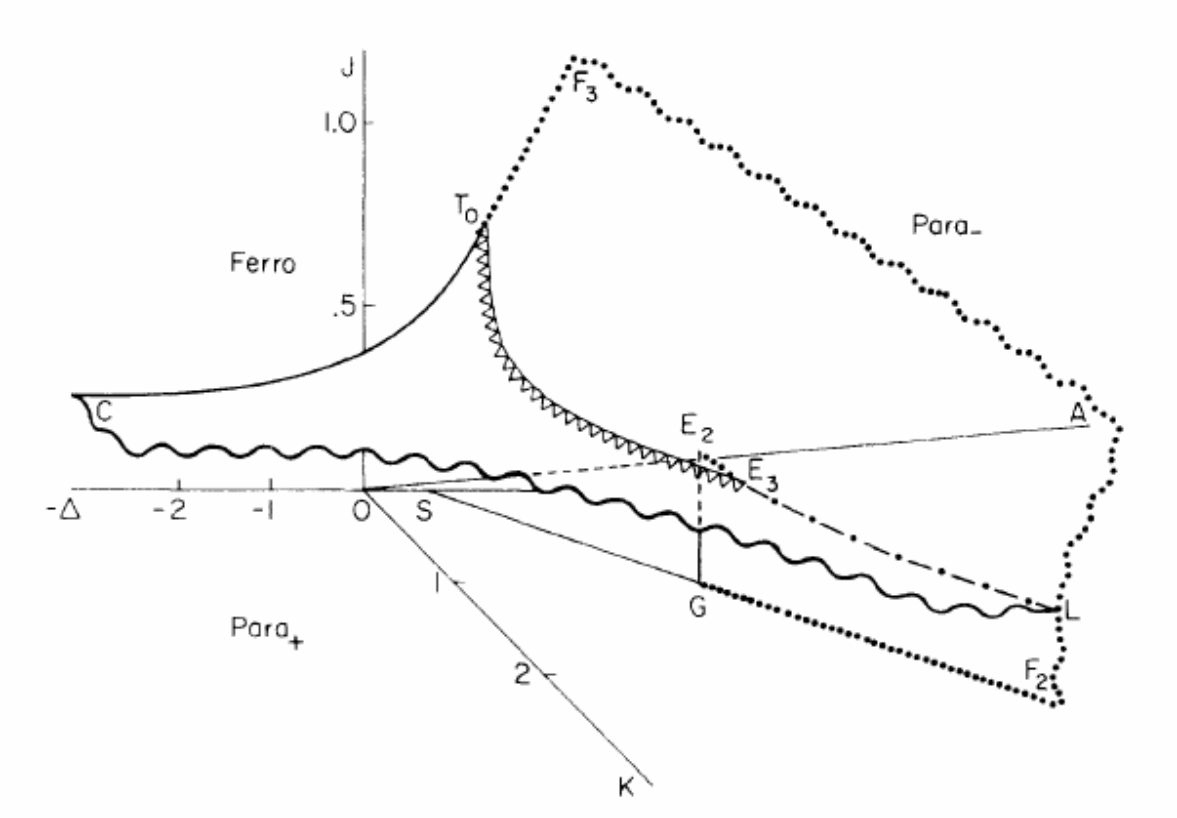

Figure 4.6: BEG phase diagram as predicted by the mean-field approximation [13]

Representative constant-K cross sections of the BEG phase diagram are shown in Figure 4.7. The solid lines represent second-order transitions; dashed lines represent first-order transitions in Figure 4.7. The ordinary tricritical points, the four-phase coexistence point, and the critical end point are, respectively, indicated by triangles, 4Φ, CEP in Figure 4.7. The second-order phase transitions line intersects the first-order transitions line at the tricritical point with same slope for different K values.

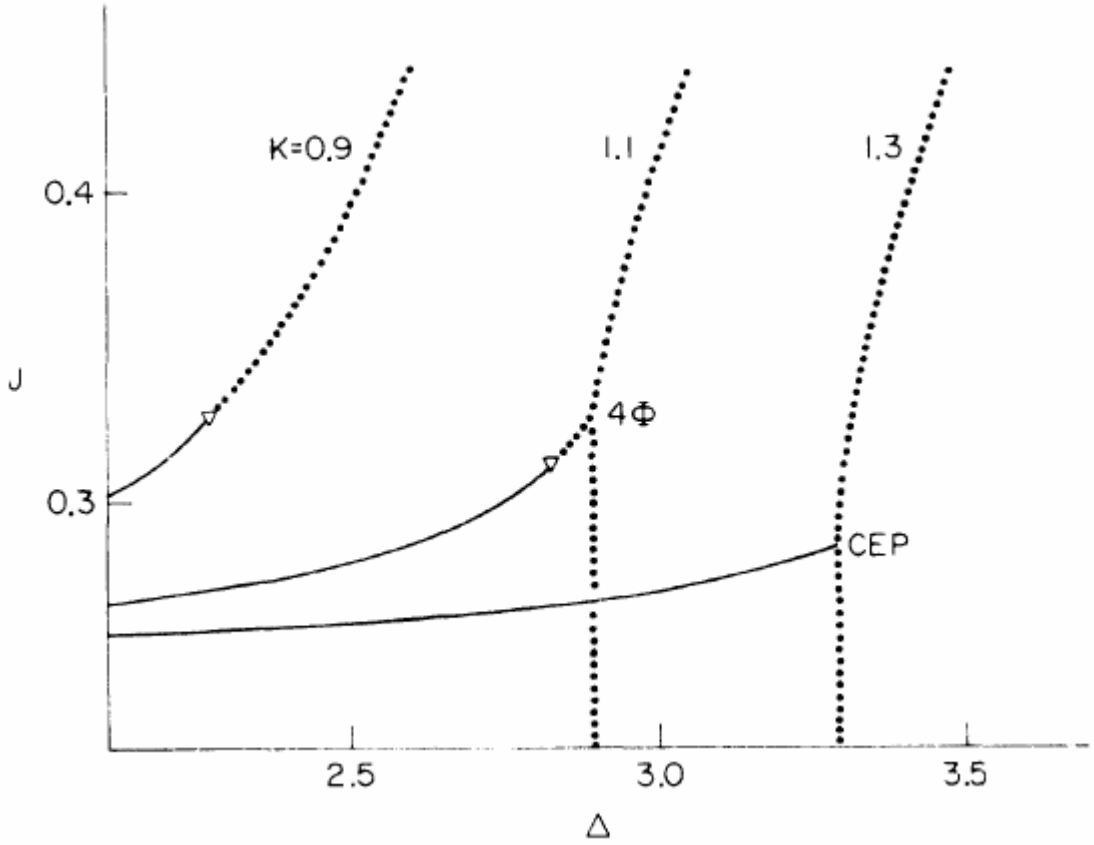

Figure 4.7: Representative constant-K cross sections of the BEG phase diagram [13].

Results of the RG theory in Case 1:

Position-space renormalization-group method gives the BEG phase diagram as shown in Figure 4.8 [13]. There are three different phases in the (J, Δ, K) space because of the effect of the positive J and K interactions. In the first region there is a coexistence of two ferromagnetic phases. If the system is in an external magnetic field, this situation causes a separation between the two ferromagnetic phases. In the other regions, there are two different types of paramagnetic phases. One of them has a large quadrupole order parameter, denoted by $Para_+$, and the other has a small quadrupole order parameter, denoted by $Para_-$ in Figure 4.8. The first-order transition surface F_2GPL separates the two paramagnetic phases $Para_\pm$. In addition there is a isolated critical line GP between these paramagnetic phases $Para_\pm$. Whereas $Para_-$ and *Ferro* are separated by the first-order transition surface F_3T_0PL, the critical transition surface CT_0PL separates $Para_+$ and *Ferro* phases. T_0P is a line of ordinary tricritical points and PL is line of critical end points. The tricritical point P which is the intersection point of the GP, PL, and T_0P lines provides the transition of the three-state Potts model. On the OA axis, the point which is shown as star gives the exact location of the Potts transition and the square point gives the location of the first-order transition obtained by MFA.

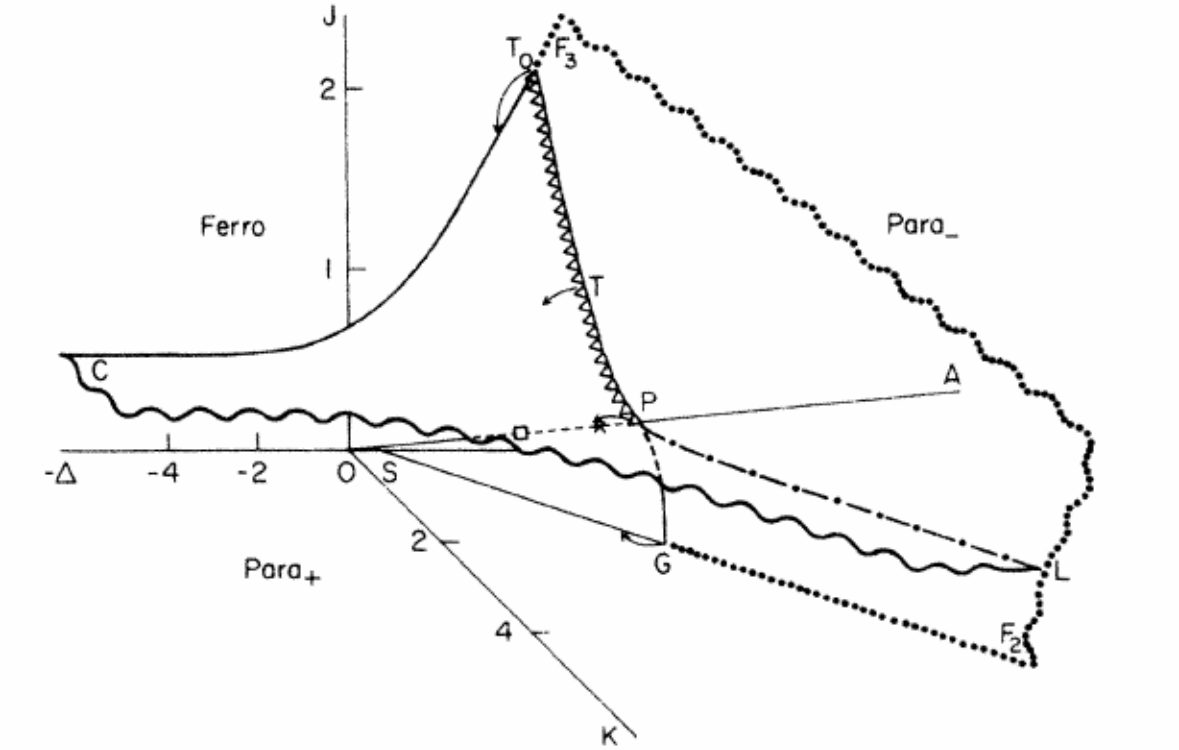

Figure 4.8: BEG phase diagram is obtained with position-space renormalization group method [13].

Representative constant-K cross sections of the BEG phase diagram, which is investigated by the PSRG treatment, is shown in Figure 4.9. In the diagrams some parts of the MFA transition lines are shown and the arrow head shows the smooth continuation of the curve. The Blume-Capel tricritical point (Δ) and the critical end point are shown. The second-order phase transitions line intersects the first-order transitions line at the tricritical point with the same slope for different K values.

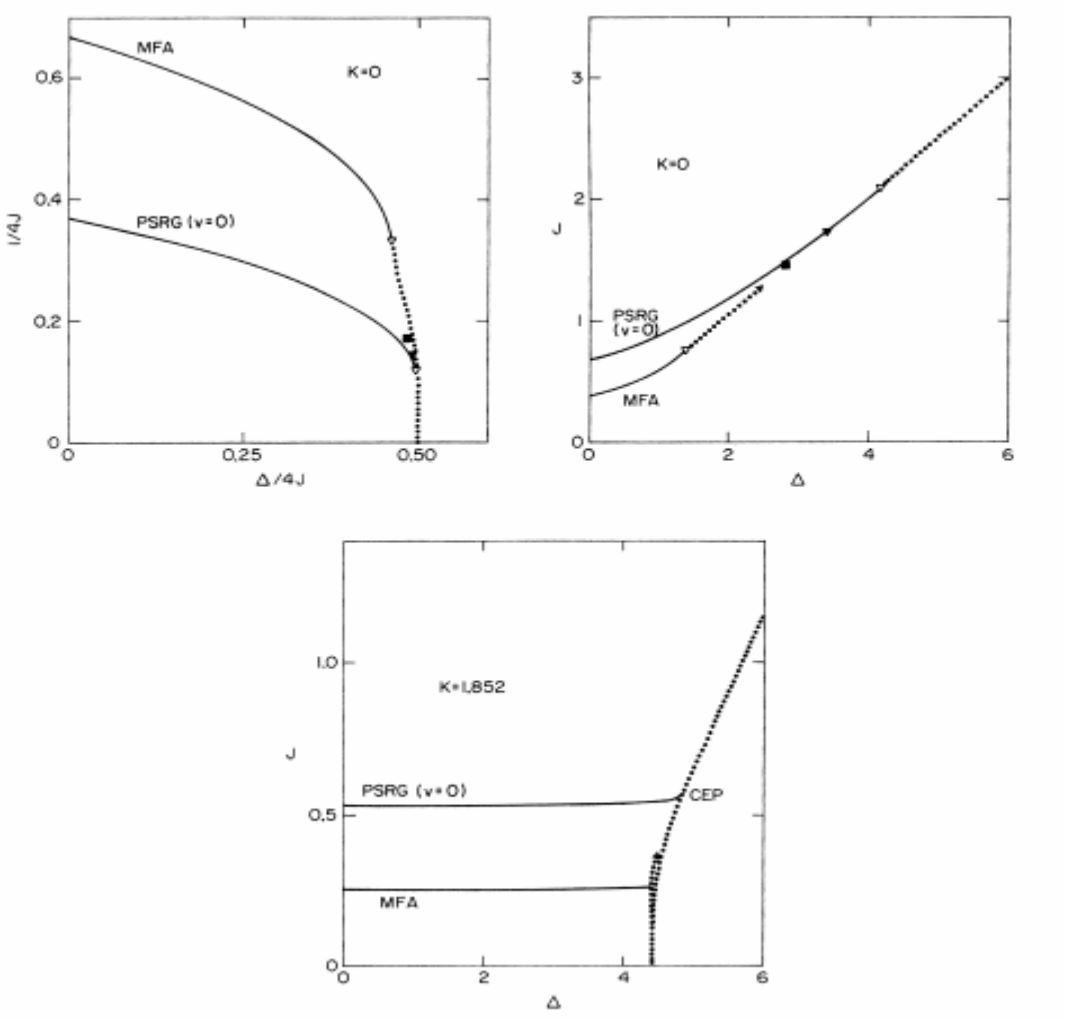

Figure 4.9: Representative constant-K cross sections of the BEG phase diagram obtained in position-space renormalization group treatment [13].

Fixed point	Type	PSRG ($v=0$) location (J^*, K^*, Δ^*)	Domain in J, K, Δ space (see Fig. 7)
	1. Higher-order fixed points		
C^*	Critical	$(0.5275, -0.1618, -\infty)$	Surface CT_0PL
G^*	Critical	$(0, 2.1100, 4.9132)$	Line GP
L^*	Critical end	$(0.5275, \infty, 2K^* + 1.0778)$	Line PL
T^*	Ordinary tricritical	$(1.1390, 0.9944, 4.2449)$	Line T_0P
P^*	Special tricritical (three-state Potts)	$(0.5822, 1.7562, 4.6779)$	Point P
	2. First-order fixed points		
Fe*	Discontinuous M	$(\infty, 0.4030 - J^*, -\infty)$ $J^*/\Delta^* = 0$	Volume Ferro
F_J^*	Discontinuous M, Q	$(\infty, \infty, 2(J^* + K^*))$ $3J^* - K^* = \infty$, $(3J^* - K^*)/\Delta^* = 0$	Portion of surface F_3T_0PL
A^*	Discontinuous M, Q	$(\infty, \infty, 2(J^* + K^*))$ $3J^* = K^*$	Line in surface F_3T_0PL
F_K^*	Discontinuous M, Q	$(\infty, \infty, 2(J^* + K^*))$ $K^* - 3J^* = \infty$, $(K^* - 3J^*)/\Delta^* = 0$	Remainder of surface F_3T_0PL
F_2^*	Discontinuous Q	$(0, \infty, 2K^* + \ln 2)$	Surface F_2GPL
	3. Trivial fixed points		
Pa_+^*	Sink for ($M=0$, large Q) phase	$(0, 0, -\infty)$	Volume Para$_+$
Pa±	Sink for ($M=0$, small Q) phase	$(0, 0, \infty)$	Volume Para$_-$
S^*	Smooth continuation between preceding two phases	$(0, 0, \ln 2)$	Surface $SGPT_0$

Table 4.1: Types and locations of the fixed points in the BEG phase diagram in Figure 4.8 [13].

The fixed points of the BEG diagram which is obtained in the position-space renormalization-group treatment is given in Table 4.1. The fixed points of the critical surface CT_0PL and the isolated critical line GP are, respectively, indicated by C^* and G^*. The results for C^* and G^* fixed points, which are given by Table 4.1, provide the properties of exact information 1 and exact information 3. Because the C^* fixed point occurs at $\Delta = -\infty$ which is in the Δ<<-1 region and the G^* fixed point occurs at J= 0 which is appropriate to the Griffiths symmetry condition, the relations between these fixed points are given by the Griffiths symmetry

$$K_{G^*} = 4J_{C^*} \text{ and } \Delta_{G^*} = 8J_{C^*} + \ln 2 . \tag{4.48}$$

The exact value of the J_{C^*} fixed point is approximately 0.4407, but the result of the calculation gives its value as 0.5275 that is 20% larger than the exact value.

The eigenvalues of the two critical fixed points C^* and G^* are given in Table 4.2. The eigenvalues λ of the recursion matrix T and the critical exponents are connected with each other by $\lambda_i = b^{y_i}$, i=2, 4,6 where the length scaling factor b is 2 in this study. Because of the Griffiths symmetry, $y_{2C} = y_{2G} = y_{2L}$ and $y_{1C} = y_{4G} = y_{1L}$. These are the thermal and magnetic eigenvalues of the Onsager critical transition.

	PSRG ($v=0$)	G^* PSRG ($v\neq 0$)	Exact [a]	C^* PSRG ($v=0$)	Exact [a]	L^* PSRG ($v=0$)
y_2	0.7267	0.9419	1	0.7267	1	0.7267
y_4	1.9416	1.8697	1.875	−1.0492		2
y_6	−1.8338	−1.6375		−∞		−∞
y_1	0.5748	0.6628		1.9416	1.875	1.9416
y_3	−0.7327	−0.6731		0.3792		0.2355

Table 4.2 The eigenvalues of the two critical fixed points C^* and G^* [13].

The critical surface CT_0P intersects the first-order surface (three-phase coexistence) F_3T_0P at the tricritical line T_0P with same slope in Figure 4.8. The position of the K=0 (Blume - Capel) tricritical point T_0, and the tricritical eigenvalues are shown in Table 4.3 [13]. There are some other results of different studies for comparison. These results are shown under the "Other PSRG" title. The results of W. Burkhardt's study [23] and B. Nienhuis and M. Nauenberg's study [24] are respectively given by "a" and "b" in Table 4.3. In addition the tricritical eigenvalues in the momentum-space renormalization-group studies [25-28] are shown in Table 3, denoted by "c". Besides the results of the Monte Carlo study of the two-dimensional BEG model, which is obtained by B. L. Arora and D. P. Landau [29], are indicated by "d" in Table 4.3.

	PSRG ($v=0$)	PSRG ($v\neq 0$)	Other PSRG [a, b]		$\epsilon \equiv 3-d$ expansion, [c] Monte Carlo [d]
y_{2T}	1.9201	1.8373	1.7966 [a]	1.852 [b]	$2-\frac{4}{125}\epsilon^2=1.968$ [c]
y_{4T}	0.7192	0.9181	0.7983 [a]	0.652 [b]	$1+\frac{1}{5}\epsilon=1.2$ [c]
y_{6T}	−0.6654	−0.6875			$-2\epsilon=-2$ [c]
y_{1T}	1.9707	1.9296	1.9275 [a]		$\frac{5}{2}-\frac{1}{2}\epsilon-\frac{1}{1000}\epsilon^2=1.999$ [c]
y_{3T}	0.6785	0.8683	1.1063 [a]		$\frac{3}{2}+\frac{3}{10}\epsilon=1.8$ [c]
J_{T_0}	2.0960	1.7317	1.724 [a]		1.5 [d]
Δ_{T_0}	4.1689	3.4127	3.400 [a]		2.8 [d]

Table 4.3: The K=0 (Blume-Capel) tricritical point and the tricritical eigenvalues [13]

The ordinary tricritical exponents are shown in Table 4.4. The equations between the critical exponents are given in Table 4.4. In this equations the lattice dimensionality d=2. The "c" and "d" marks indicates, respectively, the results of the Monte Carlo study of the two-dimensional BEG model and the Monte Carlo study of the two-dimensional spin-1/2 Ising antiferromagnet.

		Exponents		
Singular behavior [a]	Relation to eigenvalues [b]	PSRG ($v \neq 0$)	Monte Carlo [c,d]	MFA
$M \sim \tau^{\beta}_{2t}$	$\beta_t = (d - y_{1T})/y_{2T}$	0.0383	0.09 ± 0.12 [c]	$\frac{1}{4}$
$\chi \equiv \frac{\partial M}{\partial H} \sim \tau_2^{-\gamma_t}$	$\gamma_t = (2y_{1T} - d)/y_{2T}$	1.0119	1.0 ± 0.3 [c] 1.1 ± 0.4 [c]	1
$M \sim h_1^{1/\delta_t}$	$\delta_t = y_{1T}/(d - y_{1T})$	27.40	10.8 ± 0.7 [c]	5
$Q_{\text{ferro}} - Q_{\text{para}} \sim \tau_4^{\omega_u}$	$\omega_u = (d - y_{2T})/y_{4T}$	0.177	0.65 ± 0.10 [c] 0.58 ± 0.11 [d]	1
$Y \equiv \frac{\partial Q}{\partial \Delta} \sim \tau_2^{-\lambda_t}$	$\lambda_t = (2y_{2T} - d)/y_{2T}$	0.911	0.53 ± 0.14 [d]	$\frac{1}{2}$

Table 4.4: Ordinary tricritical exponents [13]

4.3.2 Three-State Potts Model

To investigate the transition of the Potts model, first of all the Hamiltonian of the system must be studied and this time the odd interactions must also be considered. The Hamiltonian of the BEG model with both even and odd interactions can be written

$$\mathrm{H}(J,K,\Delta,H,L;\{s\}) = J\sum_{<ij>} S_i S_j + K\sum_{<ij>} S_i^2 S_j^2 - \Delta\sum_i S_i^2 + H\sum_i S_i + L\sum\left(S_i S_j^2 + S_j S_i^2\right) \tag{4.49}$$

where <ij> indicates summation over nearest neighbor pairs and $S_i = \pm 1,0$.

The partition function is conserved when $S_i \to -S_i$ because of the up-down symmetry,

$$Z(J,K,\Delta,H,L) = Z(J,K,\Delta,-H,-L). \tag{4.50}$$

To calculate the relations between the interactions of the system, a new spin u_i can be defined corresponding to the general spin S_i of the system. The relation between the u_i and S_i can be written

$$u_i \equiv 1 + \frac{1}{2}S_i - \frac{3}{2}S_i^2. \tag{4.51}$$

According to this relation, the properties of the system do not change due to the transformation from S_i to u_i because the values of the new spin u_i are again +1, 0,-1. The equality of the partition function can be derived by this relation;

$$Z(J,K,\Delta,H,L) = Z(\tilde{J},\tilde{K},\tilde{\Delta},\tilde{H},\tilde{L}), \tag{4.52.a}$$

where

$$\tilde{J} = \frac{1}{4}(J + K - 2L), \tag{4.52.b}$$

$$\tilde{K} = \frac{1}{4}(9J + K + 6L), \tag{4.52.c}$$

$$\tilde{\Delta} = \frac{1}{2}\left(3qJ + qK - \Delta + 3H + 4qL\right), \tag{4.52.d}$$

$$\tilde{H} = \frac{1}{2}(qJ - qK + \Delta + H), \tag{4.52.e}$$

$$\tilde{L} = \frac{1}{4}(-3J + K + 2L), \tag{4.52.f}$$

and q is the number of nearest neighbors of a spin. For a square lattice q=4. According to these relations, any point, which is located in the (J, K, Δ, H, L) space, can be described in the $(\tilde{J}, \tilde{K}, \tilde{\Delta}, \tilde{H}, \tilde{L})$ space. The most interesting point of this situation is the one which gives the properties of the OA line in Figure 4.8. On the OA line of the BEG diagram which is shown in Figure 4.8, the interactions are connected with each other as the following equations,

$$\mathrm{K} = 3\mathrm{J}\ ,\ \Delta = 2\mathrm{qJ} = 8\mathrm{J},\ \mathrm{H} = \mathrm{L} = 0\ . \tag{4.53}$$

On this line each point maps onto itself. Due to the equation 4.53, the Hamiltonian can be rearranged as

$$\mathrm{H} = R\sum_{<ij>}\left(\delta_{S_i S_j} - 1\right), \tag{4.54}$$

where $\delta_{S_i S_j}$ is the Kronecker δ. The distance along the line from the zero-interaction origin is indicated by R and for J>0 its value is

$$R = \sqrt{\frac{2}{37}}\left(J^2 + K^2 + \Delta^2\right)^{1/2}. \tag{4.55}$$

This is the Hamiltonian of the three-state Potts model.

4.3.3 MFA prediction for the three-state Potts model

BEG phase diagram as predicted by mean-field approximation is shown in Figure 4.6. The Potts model is completely disordered at R=0 in the Potts axis OA of the BEG diagram.

This disordered phase finishes at the intersection point R_{MFA} of the Potts axis and the four-phase coexistence line E_2E_3. The location of the intersection point R_{MFA} is

$$R_{MFA} = \frac{4}{q}\ln 2 = \ln 2\,. \tag{4.56}$$

There is only ordered phases coexistence beyond R_{MFA} and the first-order surface $F_3T_0E_3L$ includes Potts axis, shown in Figure 4.6. However the results of the mean-field approximation for the Potts model are very different from the exact results which are calculated by Potts [30]. According to the study on the square lattice for the Potts model, the exact value is

$$R_{exact} = \ln(1+\sqrt{3}) \cong 1.0051 \tag{4.57}$$

so there is approximately 31% difference between the results of MFA and exact value.

4.3.4 PSRG results for the three-state Potts model

According to the position-space renormalization-group treatment calculations, the location of the Potts transition point $P*$ is at the intersection point of the ordinary tricritical line, the isolated critical line, and the critical end line in Fig. 4.8. Because of this situation, in Fig. 4.6 the four-phase coexistence line E_2E_3, which is obtained with mean-field approximation, can be found as a special tricritical point by PSRG treatment.

For the Potts model, the distance R can be calculated by the location of $P*$ in Table 4.1 so R is equal to $R_0 = 1.1696$ in PSRG$(v=0)$ and $R_v = 1.001535$ in PSRG$(v \neq 0)$. However the exact value for the Potts model is $R_{exact} = 1.005053$.

The eigenvalues of the Potts special tricritical point are given in Table 4.5. There are some results of other studies for the purpose of comparison with PSRG results. The findings of the study for two-dimensional three-state Potts model [31] is given in Table 4.5 and denoted by “a”. The “b” index in Table 4.5 refers to the Migdal’s method for Potts model.

	PSRG ($v=0$)	PSRG ($v\neq 0$)	Other PSRG [a]	$\epsilon \equiv d-1$ expansion [b]
y_{2P}	1.9416	1.8704	1.8715 [a]	$1+\epsilon=2$ [b]
y_{4P}	0.8327	1.1063	1.1806 [a]	$\epsilon=1$ [b]
y_{6P}	0.4645	0.5248	0.4570 [a]	
y_{1P}	1.9362	1.8692		
y_{3P}	0.3846	0.5304		

Table 4.5 Potts special tricritical eigenvalues [13]

The eigendirections show some important physical features of the Potts transition in PRSG. The eigendirection of y_{2P} indicates an external field coupling for the order parameter Q, because it is approximately in the direction of the Δ axis. The eigendirection of y_{4P} is almost in the direction of the Potts axis so this is related to the temperature of the Potts system. According to the PRSG results;

$$(v_J, v_K, v_\Delta) = (0.13,\ 0.34,\ 0.93) \ \text{ for PRSG } (v=0),$$
$$(v_J, v_K, v_\Delta) = (0.15,\ 0.32,\ 0.93) \ \text{ for PRSG } (v\neq 0),$$

the exact Potts axis is (0.12, 0.35, 0.93).

The Potts exponents which are obtained from these eigenvalues are shown in Table 4.6. In addition the results for low- and high-temperature series analysis [32, 33] are, respectively, indicated by c and d.

Singular behavior [a]	Relation to eigenvalues [b]	Exponents PSRG ($v \neq 0$)	Series [c,d]
Specific heat $\sim \tau_4^{-\alpha_p}$	$\alpha_p = 2 - d/y_{4P}$	0.192	0.05 ± 0.10 [c]
$Q_{\text{aligned}} - Q_P \sim \tau_4^{\beta_p}$	$\beta_p = (d - y_{2P})/y_{4P}$	0.117	0.10 ± 0.01 [c]
$\frac{\partial Q}{\partial \Delta} \sim \tau_4^{-\gamma_p}$	$\gamma_p = (2y_{2P} - d)/y_{4P}$	1.574	1.5 ± 0.2 [c] 1.42 ± 0.05 [d]
$\frac{\partial^2 Q}{\partial \Delta^2} \sim \tau_4^{-(\gamma_p + \Delta_p)}$	$\Delta_p = y_{2P}/y_{4P}$	1.691	1.58 ± 0.15 [d]

Table 4.6 Potts special tricritical exponents [13].

4.3.5 Case 2: Phase diagrams for the negative values of J and K interactions

After the study of positive values of J and K interactions of the BEG model, the negative values are searched by A. N. Berker and W. Hoston [19]. In this case, phase diagrams of the BEG model are investigated for negative values of J and K. Actually, the calculations for negative values of J are not different from the results of the positive values. Because changing the definition of the spin direction on one sublattice, which means that a transformation from J to –J, does not make any difference for the BEG model. Therefore the interesting points of this case can be observed from the phase diagrams with negative K values.

The Gibbs variational principle for the free energy,

$$F \leq \mathrm{Tr}\rho H + \beta^{-1}\mathrm{Tr}\rho \ln \rho , \tag{4.58}$$

where ρ is any density matrix which is Hermitian, non-negative, and normalized.

After minimizing the right side of this equation for the most general density matrix, there are four order parameters of the system for the resulting phases. These order parameters are,

$$\mathrm{M}_A = \langle S_i \rangle_A, \qquad \mathrm{M}_B = \langle S_i \rangle_B, \qquad Q_A = \langle S_i^2 \rangle_A, \qquad Q_B = \langle S_i^2 \rangle_B, \qquad (4.59)$$

where A and B shows the two sublattices of the system.

The global phase diagrams, which are obtained with mean field approximation, for different K/J values are shown in Figure 4.10. The disordered phase (d), ferromagnetic phase (f), ferrimagnetic phase (i), and antiquadrupolar phase (a) are shown in the phase diagrams in Figure 4.10. The first three diagrams are for positive values of K/J. For large positive value of K/J, for example Figure 4.10(a), a first order line, which comes to an end at a critical point C, and a second order transition line intersect at a critical end point E. For values of K/J close to zero, Figure 4.10(c), there are only disordered and ferromagnetic phases in the phase diagram and the second-order transition meets a first order transition line at a tricritical point. There is a different phase diagram topology between these diagrams, for example Figure 4.10(b). In this topology, there are a tricritical point T, a triple point R, and a critical point C between the disordered and ferromagnetic phases.

For K/J <0 six new type of phase diagrams are observed by mean-field theory [19]. Two of the phase diagrams are new ordered phases, a high-entropy ferrimagnetic phase and an antiquadrupolar ordered phase [19]. For negative values of K/J, for example Figure 4.10(d), first of all the tricritical point T occurs at a lower temperature. The stability limit of the tricriticality is $K/J = 1/\sqrt{10} - 1/2 \approx -0.18$, at this value the topology of the Figure 4.10(d) ends. For instance the phase diagram in Figure 4.10(e) a first order transition line is observed inside the ferromagnetic phase and terminates at the new critical point C'. Besides this first order line and the second order line in Figure 4.10(e) intersects at the new critical end point E'.

As K/J approaches -1, the new first order line and the new critical point, which appear inside the ferromagnetic phase, get smaller and at K/J= -1 value, which is shown in Figure 10(f), they disappear. There is only a second order phase transition line in the phase diagram of the K/J=-1 value, shown in Figure 4.10(f). This line has a zero-temperature critical point Z.

For the global phase diagrams of K/J<-1, the two new phases occurs. First of all, a ferrimagnetic phase, which can be described by nonzero magnetization and sublattice symmetry breaking, appears. The properties of the ferrimagnetic phase are,

$$\mathrm{M}_A \neq \mathrm{M}_B \neq 0 \qquad \text{and} \qquad Q_A \neq Q_B . \tag{4.60}$$

The antiquadrupolar phase is characterized by zero magnetization and sublattice symmetry breaking:

$$\mathrm{M}_A = \mathrm{M}_B = 0 \qquad \text{and} \qquad Q_A \neq Q_B . \tag{4.61}$$

For -1> K/J >-3 values there are two second order phase transition lines. The first one separates ferromagnetic phase and disordered phase and the other one separates the antiquadrupolar phase and disordered phase. These lines meet at a bicritical point B. There is a first-order transition between the non-zero magnetization phases and the antiquadrupolar phase, and this first-order transition line ends at the bicritical point. In addition the second-order phase transition line between the ferromagnetic and ferrimagnetic phases terminates at the critical end point E'' on the first-order line. This topology of the phase diagram is shown in Figure 4.0(g).

At K/J = -3, the critical end point E'' and the bicritical point B join at a new multicritical point A, where the three critical lines and the first order line intersect, shown in Figure 4.10(h).

Along the first order line which occurs at $\Delta / zJ = -2$ in Figure 4.10(h), the BEG model gives the properties of the antiferromagnetic three-state Potts model with the Hamiltonian;

$$-\beta H = -3J \sum_{<ij>} \delta_{S_i S_j} , \qquad J > 0 , \tag{4.62}$$

where $\delta_{S_i S_j} = 1$ for $S_i = S_j$ and $\delta_{S_i S_j} = 0$ for $S_i \neq S_j$.

For K/J < -3, in Figure 4.10(i), the multicritical point A disappears and a tetracritical point M occurs at the intersection point of the four second-order transition lines. These second order phase transition lines meet with different slopes. There is another tricritical point T'' between the ferromagnetic and antiquadrupolar phases. This time the tricriticality is observed inside the ordered phases. If K/J gets more negative values, this tricritical point occurs at lower temperatures.

In addition the phase diagrams of the different K/J values in temperature versus density are shown in Figure 4.11.

The solid lines represent a second-order phase transition and the dashed lines indicate a first-order phase transition. The special points on the phase diagrams are critical (C,C'), critical end point (E,E',E''), zero-temperature critical point (Z), zero-temperature highly degenerate (S), bicritical (B), tricritical (T,T''), tetracritical (M), multicritical (A), and triple (R).

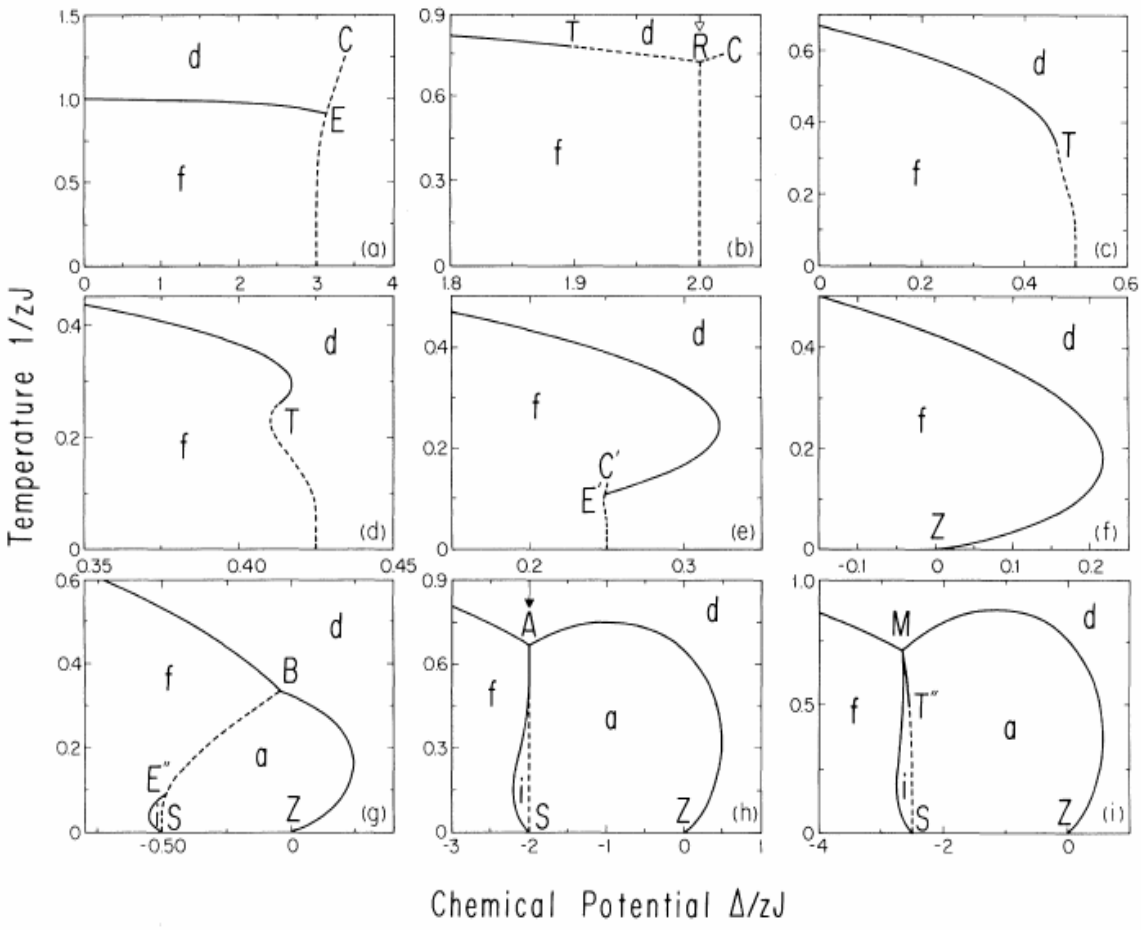

Figure 4.10: Phase diagrams for different K/J values: a) K/J = 5, b) K/J = 3, c) K/J = 0, d) K/J = -0.15, e) K/J = -0.5, f) K/J = -1, g) K/J = -1.5, h) K/J = -3, i) K/J = -3.5 [19].

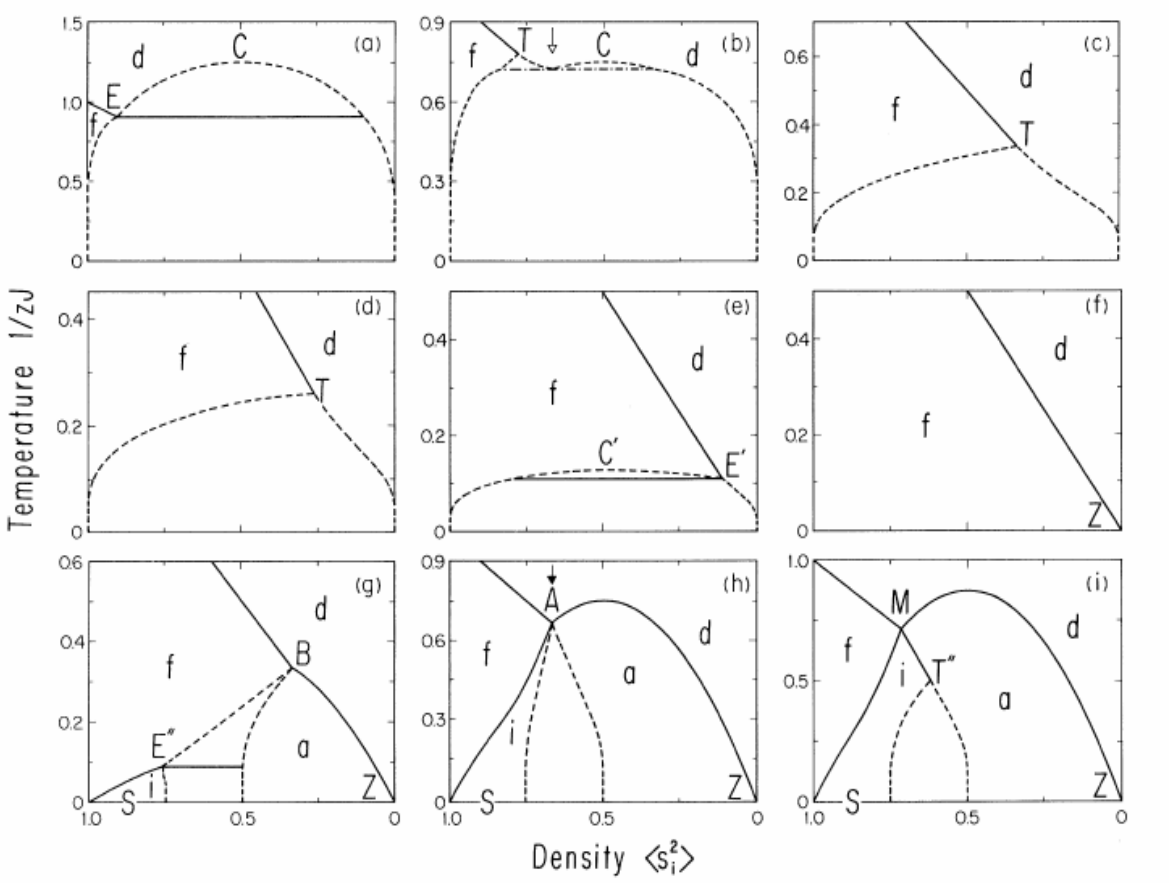

Figure 4.11: Phase diagrams in temperature and density corresponding to Figure 4.10 [19].

After that the BEG model is studied on the $He^3 - He^3$ solid-liquid-gas systems [14-16], multi-component fluid and liquid crystal mixtures [14-16], microemulsions [17], and semiconductor alloys [18].

Stepwise Positional and Orientational Ordering in the Spin-3/2 Ising Model: A Plastic Crystal Phase Diagram from Renormalization-Group Theory

The spin-3/2 Ising model with nearest-neighbor interactions exhibits intricate but physically suggestive phase diagrams, as for example shown in Figure 5.1 including three separate ferromagnetic phases and a positionally ordered phase, new special points, and a temperature sequence of stepwise positional and orientational ordering as in plastic crystals. Other phase diagram cross-sections include order-order critical points and unusual bicritical points.

The Hamiltonian of the spin-1/2 Ising model is

$$-\beta H = J\sum_{<ij>} S_i S_j \,, \tag{5.1}$$

where each spin $S_i = \pm 1/2$ and the sum is over all pairs of nearest-neighbor sites, generalizes for the spin-1 Ising model to

$$-\beta H = \sum_{<ij>} \left[JS_i S_j + KS_i^2 S_j^2 - \Delta\left(S_i^2 + S_j^2\right)\right], \tag{5.2}$$

where $S_i = \pm 1,0$ [12]. Equation 5.2 constitutes the most general spin-1 Ising model with nearest-neighbor interactions only and no externally imposed symmetry breaking in the ordering degrees of freedom. The global solution of the spin-1 Ising model played an important role through applicability to the many physical systems that incorporate non-ordering degrees of freedom ($S_i = 0$, where i is a site index) as well as ordering degrees of

freedom ($S_i = \pm 1$) [12, 13, 19]. The next qualitative step is the global study of a model system that has two different types of local ordering degrees of freedom, the spin-3/2 Ising model [34-51]:

$$-\beta \mathrm{H} = \sum_{<ij>} \{(J + LP_iP_j + MQ_iQ_j)S_iS_j + K(P_iP_j + Q_iQ_j) - \Delta(S_i^2 + S_j^2)\} \qquad (5.3)$$

where <ij> indicates summation over all nearest-neighbor in lattice model and at each site on the lattice, the spin can be ±3/2 or ±1/2. This is the most general spin-3/2 Ising model with only nearest-neighbor interactions and no externally imposed symmetry breaking in the ordering degrees of freedom. The projection operators in eq 5.3 are $P_i = 1 - Q_i = 1,0$ for $S_i = \pm 3/2, \pm 1/2$ respectively.

Of the models defined above, the spin 1/2 Ising model has a single critical point on the temperature J^{-1} axis. The spin-1 Ising model, in the temperature and chemical potential Δ / J plane, has three different types of phase diagrams when the biquadratic interaction K is non-negative [13]. When negative biquadratic interactions are considered, nine more different types of phase diagrams are obtained from mean-field theory [19].

In this study on the spin 3/2 Ising model, using renormalization group theory, an extraordinarily rich solution is obtained with 6 different types of phase diagrams and 4 different ordered phases, exhibiting first-order phase transitions between variously ordered phases, critical points imbedded within ordered phases, and a variety of multicritical points.

The Hamiltonian of equation 5.3 is expressed as $-\beta H = \sum_{<ij>} -\beta H_{ij}$ and the transfer matrix is the exponentiated nearest-neighbor Hamiltonian, $-\beta H_{ij}$. The renormalization-group treatment of the system, for spatial dimension d and length-rescaling factor b, is effected by taking the b th power of the transfer matrix and then by taking the b^{d-1} nth

power of each term of the resulting matrix, to obtain the transfer matrix of the renormalized system. Repetition of this procedure gives the renormalization-group flows in 5-dimensional Hamiltonian space (J, L, M, K, Δ). This treatment constitutes an approximate solution for hypercubic lattices and an exact solution for hierarchical lattices [52-62]. Thus, the spin-3/2 Ising model is studied in spatial dimension d=2 with length rescaling factor b=2, obtaining the global phase diagrams, which is underpinned by 32 renormalization-group fixed points.

In this study, one of the ordering species is $|S_i| = 3/2$, the other one is $|S_i| = 1/2$. The chemical potential Δ / J controls the relative amounts of each ordering species. The "biquadratic" interaction, the term with dimensionless coupling strength K in equation (5.3), controls the clustering of each ordering species. Figure 5.2, where M = L = 0, show the effects of the biquadratic interaction on the global phase diagram. The temperature versus chemical potential phase diagram for large K / J (dividing out temperature), where clustering is favored, is illustrated in Figure 5.2(e) and 5.2(f) with $K / J = 5$ and $K / J = 10$: In these phase diagrams, two ferromagnetically ordered phases are seen at low temperatures, each rich in one of the ordering species. Upon increasing temperature, each ferromagnetic phase undergoes a second-order transition to the paramagnetic (disordered) phase that is rich in the corresponding species. By changing the chemical potential Δ / J, a first-order phase transition is induced between phases rich in different species, namely between the two ferromagnetic phases at low temperatures, between a ferromagnetic phase and the opposite paramagnetic phase at intermediate temperatures, and between the two paramagnetic phases at higher temperatures. The first-order transitions between the paramagnetic phases terminate at a critical point. Each second-order phase transition line between a ferromagnetic and the corresponding paramagnetic phases abuts at a critical end point on the chemical potential induced first-order transition boundary.

As the biquadratic coupling strength K / J is decreased from large positive values, the critical point and the two critical end-points approach each other and merge. For smaller K / J values, illustrated in Figure 5.2(d) with $K/J = 0$, the two second-order transition lines and the first-order transition line terminate at an unusual bicritical point. At a bicritical point in a field-space phase diagram as is the case here, two second-order transition lines and a first-order transition line meet tangentially. However, whereas, in bicritical points studied to date [63], the second-order lines and the first-order line are on opposite sides of the bicritical point, in the present system one second-order line is on the side of the first-order line.

As the biquadratic coupling strength K / J is made more negative, a sublattice-wise (i.e., positionally) ordered, as well as ferromagnetically (i.e., orientationally) ordered phase appears at K / J = -1/2. As illustrated in Figures 5.2(b) and 5.2(c) with $K/J = -5$ and $K/J = -15$, this phase occurs at low temperatures and intermediate chemical potentials. It is ferromagnetically ordered, with each ordering species predominantly occurring in one of the two sublattices. The transitions between the ordered phases are first order, with three lines meeting at a triple point (actually, an eight-phase coexistence point, if the degeneracies of each ordered phases are also counted). For K/J<2.2, the bicritical point is replaced by a double critical end point. The first-order transitions between the paramagnetic phases terminate at a critical point.

For even more negative values of K / J<-23.8, a portion of the sublattice ordered phase has erupted through the ferromagnetic ordering lines and in the process lost ferromagnetic ordering, as illustrated in Figure 5.1 with K / J = -50. Thus, a new phase appears, that is sublattice-wise (positionally) ordered, but paramagnetic. Each ordering species predominantly occurs in one of the two sublattices, with no preferred spin orientation. This regime offers a phase diagram topology, to the common knowledge not seen before, with multiple first- and second-order phase transitions meeting and four

different ordered phases. Two of these phases are positionally ordered, one phase is only positionally ordered, and one phase is both orientationally and positionally ordered.

At intermediate chemical potentials, as temperature is lowered, the sequence of disordered, then only positionally ordered, finally positionally and orientationally ordered phases are encountered, as in plastic crystal experimental systems.

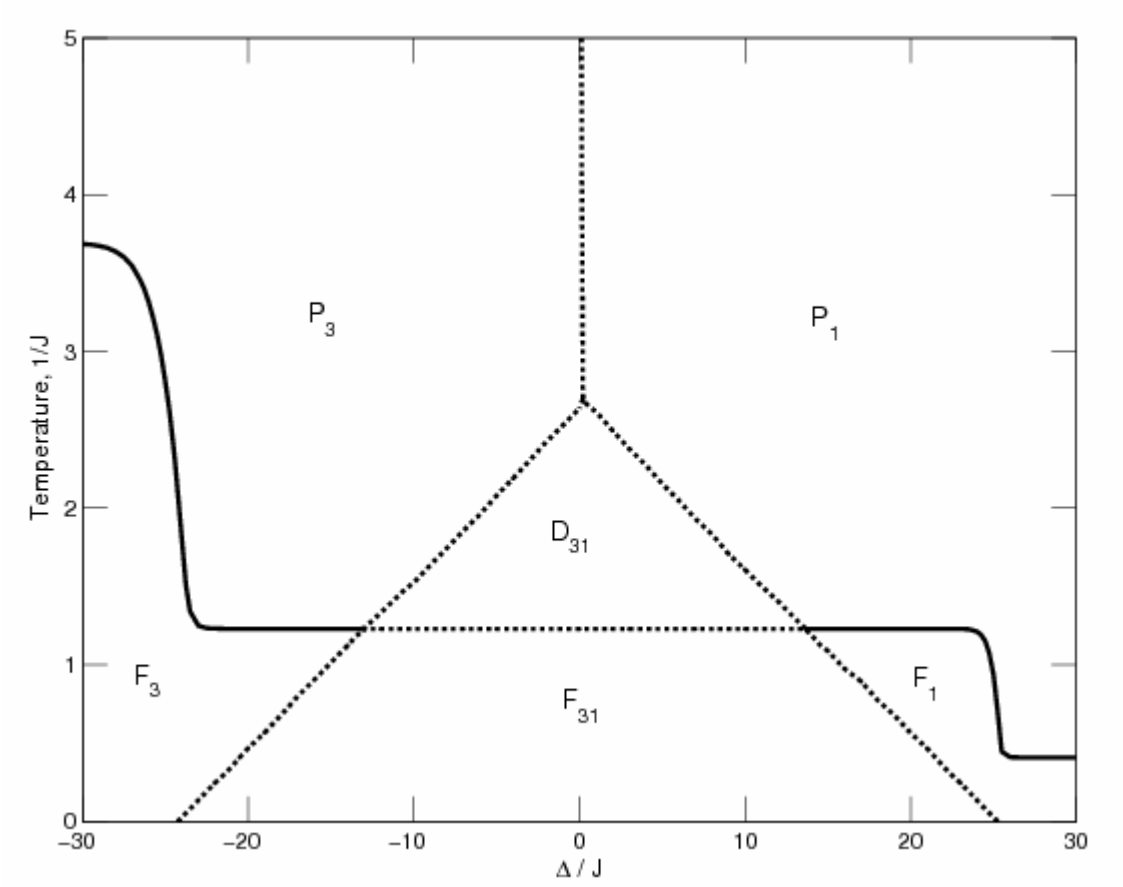

Figure 5.1: Temperature versus chemical potential phase diagram of the spin-3/2 Ising model in dimension d = 2, for K / J = -50 and L = M = 0.

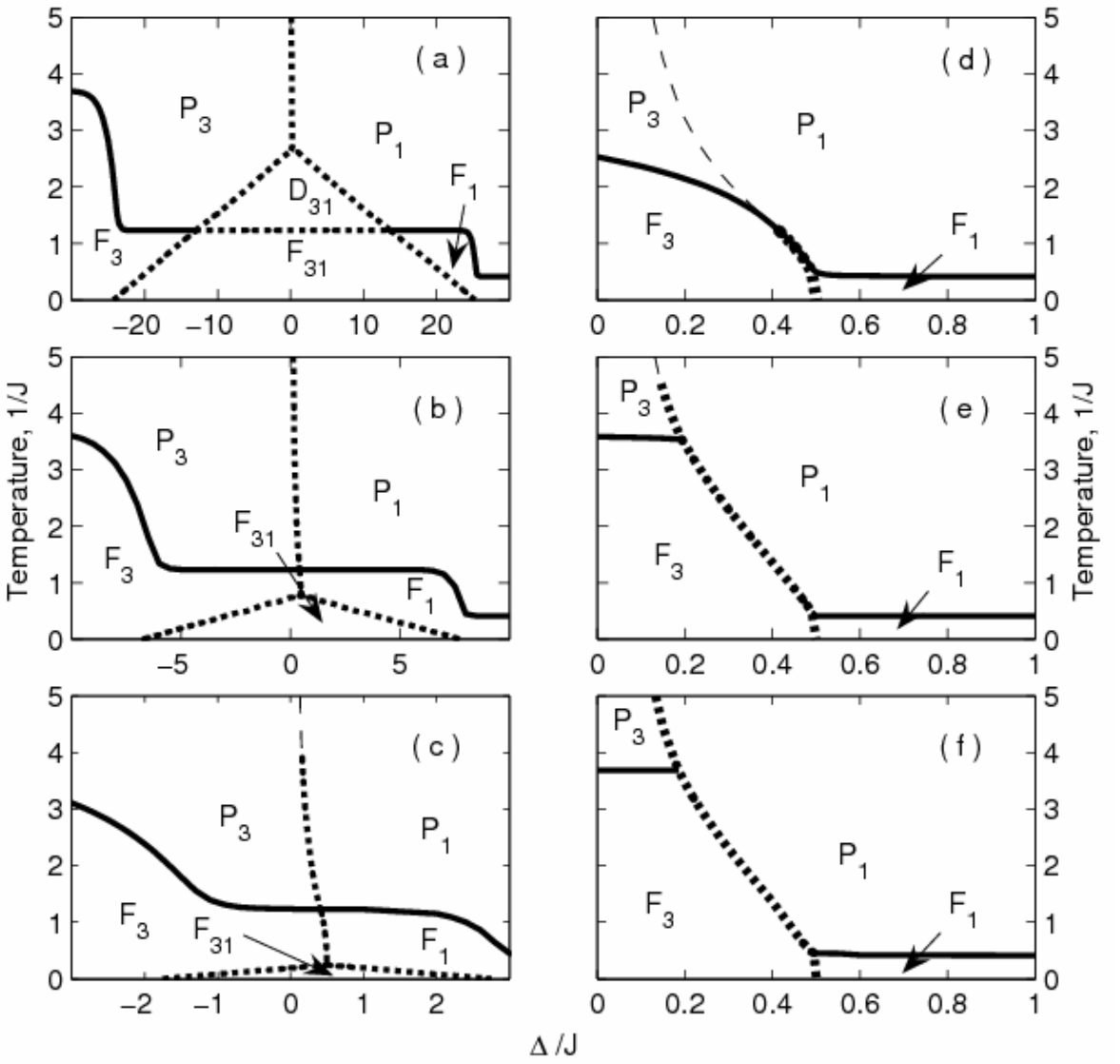

Figure 5.2: Phase diagrams for (a) K / J = -50, (b) K / J = -15, (c) K / J = -5, (d) K / J = 0, (e) K / J = 5, and (f) K / J = 10 with L = M = 0.

Another phase diagram topology is obtained, starting from Figure 5.2(d) with $K = M = 0$. As L / J is increased from zero, the first-order line detaches from the second-order lines, resulting in another new phase topology, as illustrated in Figure 5.3 with L / J = 5. The first-order phase transitions between the two ferromagnetic phases end at an isolated critical point totally embedded within ferromagnetism. Thus, a smooth passage, with no phase transition singularity, can occur between the two ferromagnetic phases. The second-order phase boundary between the ferromagnetic and paramagnetic phases exhibits a kink, although there is no phase boundary meeting it at this point. The renormalization-group mechanism for this phenomenon is a disorder-in-order (on the low temperature side) and disorder-in-disorder (on the high temperature side) supercritical line crossing this point.

Finally, it is well-known [13] that multicomponent models reduce to permutation-symmetric Potts models in subspaces of their generalized Hamiltonian space. The phase diagram containing the 4-state Potts model is in Figure 5.4. The 4-state Potts second-order transition point shows the usual bicritical topology between the ferromagnetically ordered phases.

The solid and dotted lines, respectively, indicate the second-order and the first-order transition lines. The dashed line is a disorder line smoothly mediating, with no phase transition between two phases.

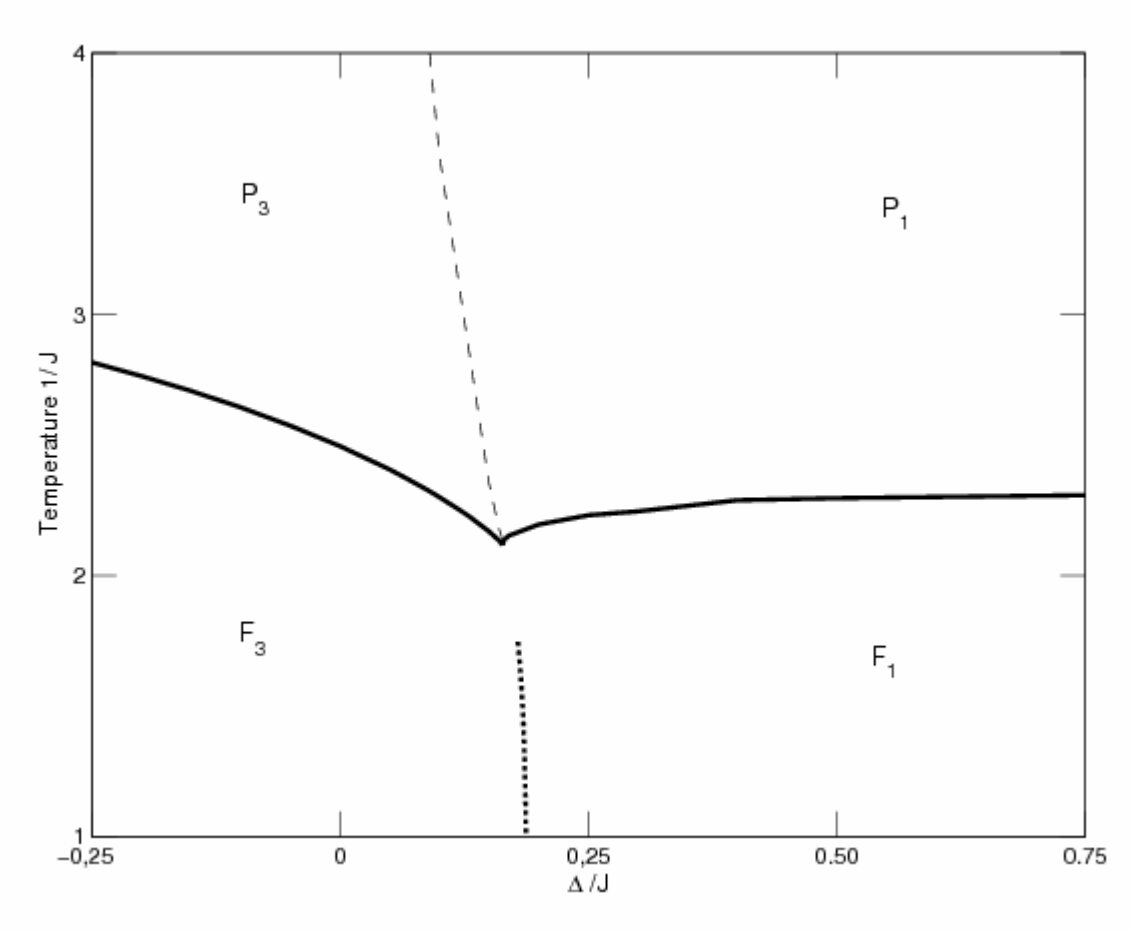

Figure 5.3: Phase diagram for L / J = 5 values with K = M = 0

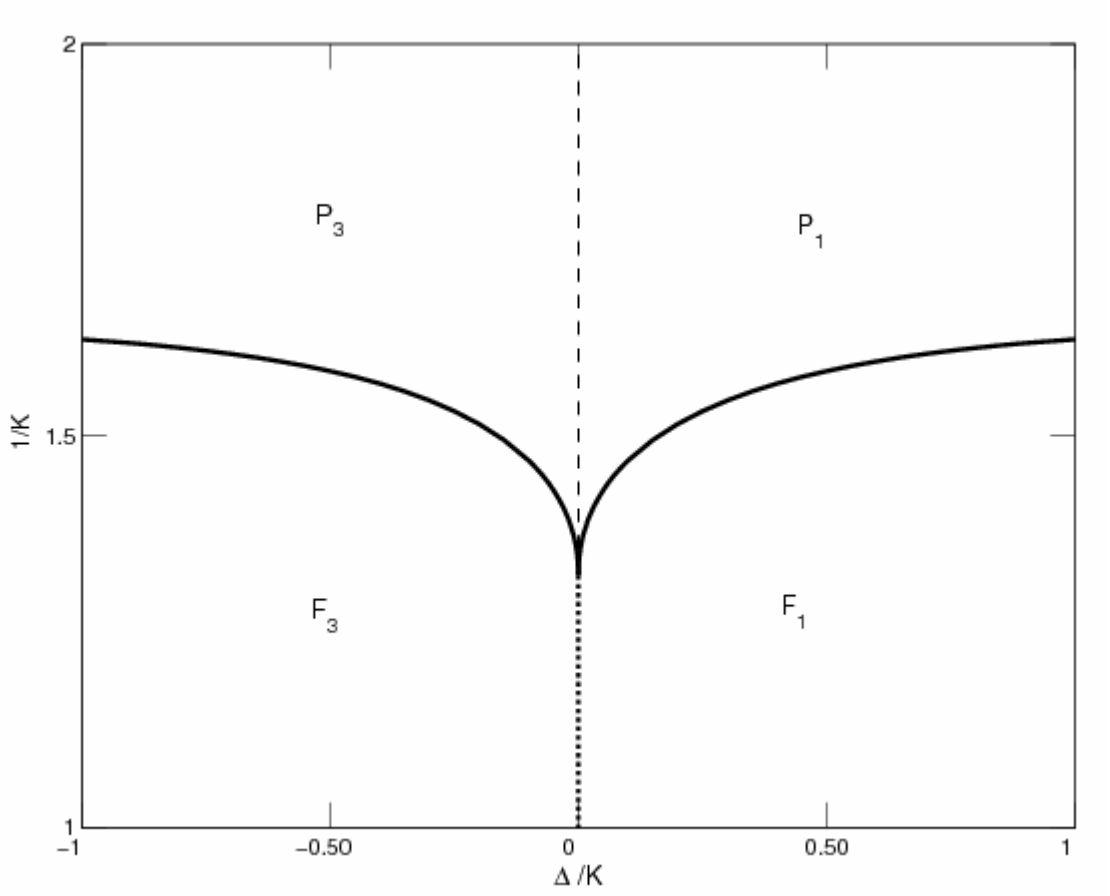

Figure 5.4: Phase diagram of the 4-state Potts model

BIBLIOGRAPHY

[1] J. M. Yeomans, "Statistical Mechanics of Phase Transitions," Oxford, Clarendon Press (1992).

[2] H. E. Stanley, "Introduction to Phase Transitions and Critical Phenomena," Oxford University Press (1971).

[3] K. Huang, "Statistical Mechanics," John Wiley & Sons, Canada (1963).

[4] D. Amit, "Field Theory, Renormalization Group and Critical Phenomena," World Scientific (1984).

[5] J. J. Binney, N. J. Dowrick, A. J. Fisher, and M. E. J. Newman, "Theory of Critical Phenomena: An Introduction to the renormalization group," Oxford University Press (1992).

[6] R. J. Creswick, H. A. Farach, and C. P. Poole, "Introduction to Renormalization Group Methods in Physics," John Wiley & Sons, Canada (1992).

[7] L. P. Kadanoff, Physics **2**, 263 (1966).

[8] K. G. Wilson, Phys. Rev. B **4**, 3174 (1971).

[9] C. Domb, "The Critical Point - A Historical Introduction to the Modern Theory of Critical Phenomena," Taylor & Francis (1996).

[10] De Gennes, P. G. , Phys. Lett. A **38**, 339 (1972).

[11] T. L. Bell, Phys. Rev. A **17**, 1049 (1978).

[12] M. Blume, V. J. Emery, and R. B. Griffiths, Phys. Rev. A **4**, 1071 (1971).

[13] A. N. Berker and M. Wortis, Phys. Rev. B **14**, 4946 (1976).

[14] J. Lajzerowicz and J. Sivardiere, Phys. Rev. A **11**, 2079 (1975).

[15] J. Lajzerowicz and J. Sivardiere, Phys. Rev. A **11**, 2090 (1975).

[16] J. Lajzerowicz and J. Sivardiere, Phys. Rev. A **11**, 2101 (1975).

[17] M. Schick and W. H. Shih, Phys. Rev. B **34**, 1797 (1986).

[18] K. E. Newman and J. D. Dow, Phys. Rev. B **27**, 7495 (1983).

[19] A. N. Berker and W. Hoston, Phys. Rev. Lett. **67**, 1027 (1991).

[20] J. Wilks, "The Properties of Liquid and Solid Helium," Clarendon, Oxford (1967).

[21] E. H. Graf, D. M. Lee, and J. D. Reppy, Phys. Rev. Lett. **19**, 417 (1967).

[22] R. B. Griffiths, Physica **33**, 689 (1967).

[23] T. W. Burkhardt, Phys. Rev. B **14**, 1196 (1976).

[24] B. Nienhuis and M. Nauenberg, Phys. Rev. B **13**, 2021 (1976).

[25] M. J. Stephen and J. L. McCauley, Jr., Phys. Rev. Lett. A **44**, 89 (1973).

[26] T. S. Chang, G. F. Tuthill, and H. E. Stanley, Phys. Rev. B **9**, 4882 (1974).

[27] G. F. Tuthill, J. F. Nicoll, and H. E. Stanley, Phys. Rev. B **11**, 4579 (1975).

[28] F. J. Wegner, Phys. Lett. A **54**,1 (1975).

[29] B. L. Arora and D. P. Landau, AIP Conf. Proc. **10**, 870 (1973).

[30] R. B. Potts, Proc. Camb. Philos. Soc. **48**, 106 (1952).

[31] C. Dasgupta, Phys. Rev. B **14**, 1221 (1976).

[32] J. P. Straley and M. E. Fisher, J. Phys. A **6**, 1310 (1973).

[33] D. Kim and R. I. Joseph, J. Phys. A **8**, 891 (1975).

[34] J. Sivardière, A.N. Berker, and M. Wortis, Phys. Rev. B **7**, 343 (1973).

[35] D. Mukamel and M. Blume, Phys. Rev. A **10**, 610 (1974).

[36] S. Krinsky and D. Mukamel, Phys. Rev. B **11**, 399 (1975).

[37] S. Krinsky and D. Mukamel, Phys. Rev. B **12**, 211 (1975).

[38] D. Furman, S. Dattagupta, and R.B. Grifftihs, Phys. Rev. B **15**, 441 (1977).

[39] E. Albayrak and M. Keskin, J. Mag. Mag. Mat. **218**, 121 (2000).

[40] C. Ekiz, E. Albayrak, and M. Keskin, J. Mag. Mag. Mat. **256**, 311 (2003).

[41] Ö. Ozsoy and M. Keskin, Physica **319**, 404 (2003).

[42] O. Canko and M. Keskin, Phys. Lett. A **320**, 22 (2003).

[43] O. Canko and M. Keskin, Phys. Lett. A **348**, 9 (2005).

[44] O. Canko and M. Keskin, Int. J. Mod. Phys. **20**, 455 (2006).

[45] O. Canko, B. Deviren, and M. Keskin, J. Phys. - Cond. Mat. **18**, 6635 (2006).

[46] M. Keskin, M. A. Pınar, A. Erdinç, and O. Canko, Phys. Lett. A **353**, 116 (2006).

[47] M. Keskin, M. A. Pınar, A. Erdinç, and O. Canko, Physica A **364**, 263 (2006).

[48] M. Keskin, O. Canko, and B. Deviren, Phys. Rev. E **74**, 011110 (2006).

[49] M. Keskin, O. Canko, and M. Kırak, J. Stat. Phys. **127**, 359 (2007).

[50] M. Keskin, O. Canko, and B. Deviren, J. Mag. Mag. Mat. **313**, L1 (2007).

[51] M. A. Pınar, M. Keskin, A. Erdinç, and O. Canko, Z. Nat. A **62**, 127 (2007).

[52] A. N. Berker and S. Ostlund, J. Phys. C **12**, 4961 (1979).

[53] R. B. Griffiths and M. Kaufman, Phys. Rev. B **26**, 5022R (1982).

[54] M. Kaufman and R. B. Griffiths, Phys. Rev. B **30**, 244 (1984).

[55] A. Erbas, A. Tuncer, B. Yücesoy, and A. N. Berker, Phys. Rev. E **72**, 026129 (2005).

[56] M. Hinczewski and A. N. Berker, Phys. Rev. E **73**, 066126 (2006).

[57] M. Hinczewski, Phys. Rev E **75**, 061104 (2007).

[58] Z. Zhang, L. Rong, and S. Zhou, Physica A **377**, 329 (2007).

[59] Z. Zhang, S. Zhou, and T. Zou, Eur. Phys. J. B **56**, 259 (2007).

[60] H. D. Rozenfeld and D. ben-Avraham, Phys. Rev. E **75**, 061102 (2007).

[61] H. D. Rozenfeld, S. Havlin, and D. ben-Avraham, arXiv: cond-mat/0612330v2 [cond-mat.stat-mech].

[62] E. Khajeh, S.N. Dorogovtsev, and J.F.F. Mendes, Phys. Rev. E **75**, 041112 (2007).

[63] A D. Bruce and A. Aharony, Phys. Rev. B **11**, 478 (1975).

[64] J. A. Pople and F. E. Karasz, J. Phys. Chem. Solids **18**, 28 (1961).